ACS BIO & MED CHEM Au
AN OPEN ACCESS JOURNAL OF THE AMERICAN CHEMICAL SOCIETY

pubs.acs.org/biomedchemau
Review

Discovery of Noncanonical Iron and 2-Oxoglutarate Dependent Enzymes Involved in C−C and C−N Bond Formation in Biosynthetic Pathways

Yaoyao Shen, Anyi Sun, Yisong Guo,* and Wei-chen Chang*

Cite This: ACS Bio Med Chem Au 2025, 5, 238−261
Read Online

ABSTRACT: Iron and 2-oxoglutarate dependent (Fe/2OG) enzymes utilize an Fe^{IV}═O species to catalyze the functionalization of otherwise chemically inert C−H bonds. In addition to the more familiar canonical reactions of hydroxylation and chlorination, they also catalyze several other types of reactions that contribute to the diversity and complexity of natural products. In the past decade, several new Fe/2OG enzymes that catalyze C−C and C−N bond formation have been reported in the biosynthesis of structurally complex natural products. Compared with hydroxylation and chlorination, the catalytic cycles of these Fe/2OG enzymes involve distinct mechanistic features to enable noncanonical reaction outcomes. This Review summarizes recent discoveries of Fe/2OG enzymes involved in C−C and C−N bond formation with a focus on reaction mechanisms and their roles in natural product biosynthesis.

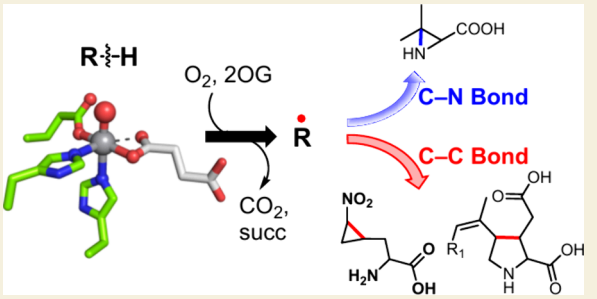

KEYWORDS: *Natural product, Oxygenase, Iron and 2-oxoglutarate dependent enzyme, Biosynthesis, C−H bond activation, C−C bond, C−N bond, Enzyme mechanism*

1. IRON AND 2-OXOGLUTARATE DEPENDENT ENZYMES

Targeted C−H bond activation leading to diverse but well-controlled outcomes has become a focal point of modern chemistry, while it still remains a challenging task in organic synthesis.[1] In Nature, metalloenzymes with different metallocofactor compositions are able to catalyze C−H bond activation with exceptional regio- and stereoselectivity. In the past two decades, iron and 2-oxoglutarate dependent (Fe/2OG) enzymes have been discovered to catalyze an ever-growing array of novel oxidative modifications of small molecules, thereby contributing to the diversity and complexity of the chemical structures seen in natural products. Compared to other metalloenzymes that utilize alternative cofactors and chemistry (e.g., cytochrome P450 and radical SAM enzymes among others), the simple requirements of ferrous iron, molecular oxygen, and 2OG make Fe/2OG enzymes ideal candidates for the development of novel biocatalysts.[2,3]

Fe/2OG enzymes are widespread and play extremely diverse roles in nature.[4−6] First, they are involved in the modification of protein in chromatin, regulation of transcription, and mRNA demethylation.[7] Additionally, Fe/2OG enzymes are known to activate inert C−H bonds resulting in diverse oxidative transformations including hydroxylation,[8−10] desaturation,[11,12] epimerization,[13] halogenation,[14−16] epoxidation,[17−21] endoperoxidation,[22] isonitrile formation,[23−26] and C−C or C−N bond formations in secondary metabolism. These oxidative reactions lead to extensive structural diversity and complexity in biosynthetic products that are critical to their biological properties.

The structures of all Fe/2OG proteins characterized to date exhibit a double-stranded β-helix (i.e., cupin) fold[27] and, with the exception of the halogenases, utilize a 2-His-1-carboxylate triad (H-X-(D/E)-Xn-H) for iron binding (Figure 1).[28] In halogenases, the D/E ligand is replaced by a G/A residue for the coordination of a halide ligand to the iron.[14,29] In nonhalogenases, the 2-His-1-carboxylate ligated ferrous (Fe^{II}) center is coordinated with three water molecules in the resting state. As the substrate , 2OG, and molecular oxygen are introduced, the reaction occurs. Henceforth, the term "substrate" refers to a target compound containing the C−H to be activated. 2OG binds to the Fe^{II} via its C1 carboxylate and C2-ketone moieties prior to subsequent coordination and reduction of molecular oxygen, resulting in an Fe^{III}-superoxo

Received: January 2, 2025
Revised: February 24, 2025
Accepted: February 25, 2025
Published: March 10, 2025

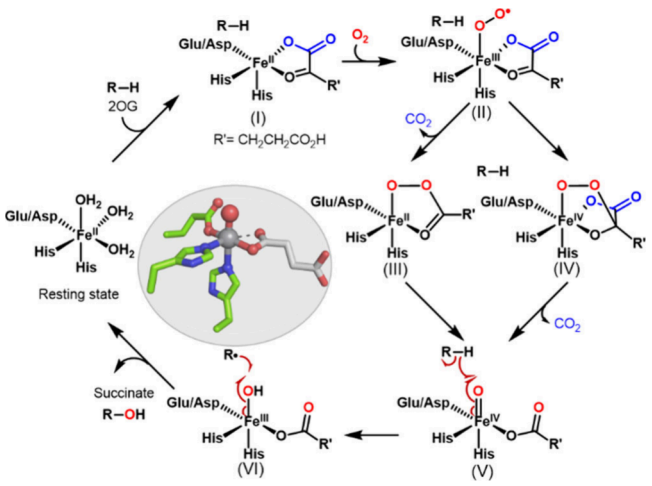

Figure 1. Catalytic cycle of Fe/2OG enzyme catalyzed hydroxylation and a vanadyl mimic of the Fe^{IV}=O species found in VioC (PDB: 6ALR).

species (I → II).[30] Release of CO_2 followed by the formation of a C−O bond between Fe^{III}-superoxo and carbonyl carbon or vice versa leads to the formation of the Fe^{IV}=O species (II → III → V or II → IV → V). This highly reactive species represents the common key intermediate of Fe/2OG enzyme chemistry that abstracts a hydrogen atom from the substrate to result in a substrate radical and Fe^{III}−OH (VI). During hydroxylation, oxygen rebound takes place to produce a hydroxylated product and regenerate Fe^{II}. Consequently, Fe/2OG enzymes catalyze a two-electron oxidation of the substrate for each equivalent of O_2 and 2OG that are converted into H_2O, CO_2, and succinate.[8,9,31−33] In halogenases, following C−H bond activation, the substrate radical can undergo either a halide or oxygen rebound pathway. Based on spectroscopic,[15,34,35] crystallographic,[14] and computational studies,[36,37] orientation of the Fe^{IV}=O moiety, position of substrate with respect to the HO−Fe−Cl/Br plane, and hydrogen bonding networks between protein residues with Fe(III)-hydroxyl and succinate are involved to facilitate halogenation outcome. Additionally, using a tyrosine residue as the hydrogen atom donor to quench the substrate radical to furnish epimerization is deployed by carbapenem synthase to invert the chirality found in carbapenem biosynthesis.[13] Interestingly, based on the protein structure, spectroscopic studies, along with mutagenesis, the resulting tyrosyl radical is distributed among a few tyrosine residues.[13]

Several studies have recently explored the chemistry behind nonhydroxylating reactions catalyzed by Fe/2OG enzymes, emphasizing the different fates of the substrate radical and Fe(III)−OH complex. In 2019, Pan et al. discovered that the oxacyclases LolO and H6H as well as the chlorinase SyrB2 have sluggish hydroxyl rebound rates, leading to the proposal that rebound is suppressed by structural and dynamical factors that facilitate nonhydroxylating reaction outcomes.[38] Recently, Wenger et al. revealed that substrate positioning and shifts in the Fe^{IV}=O···H (substrate) angle correlate with the reaction outcome (101° vs 112° corresponds to epoxidation vs hydroxylation).[21] These studies established the groundwork for understanding the intricate control that enables alternative reaction outcomes, such as oxacyclization and chlorination. However, mechanistic details on how Fe/2OG enzymes enable other types of reactions remain to be established. This Review summarizes recent discoveries and new mechanistic insights regarding Fe/2OG enzyme-catalyzed C−C and C−N bond formations observed in natural product biosynthesis.

2. C−C AND C−N BOND FORMING REACTIONS

Since the discovery of PlaO1,[39] more than a dozen Fe/2OG enzymes have been shown to catalyze C−C and C−N bond installation reactions (Figure 2). Following targeted C−H bond activation, subsequent C−C and C−N bond formation instead of hydroxylation can result in structural rearrangements as well as ring formation including the construction of cyclopropane and aziridine moieties. Therefore, Fe/2OG enzymes catalyzing these types of reactions have been found to participate in a wide range of natural product maturation processes including those of stipitatic acid,[40] preaustinoid A3,[41] berkeleydione,[42] anditomin,[43,44] deoxypodophyllotoxin,[45] cycloclavine,[46] nogalamycin,[47] kainic acid,[48] domoic acid,[49] okaramine E,[50] dehydrofosmidomycin,[51] pleurocybellaziridine,[52] 3-(2-nitrocyclopropyl)alanine,[53,54] brevione W,[55] helvamide B,[56] arizonamide,[57] and medicaol.[58]

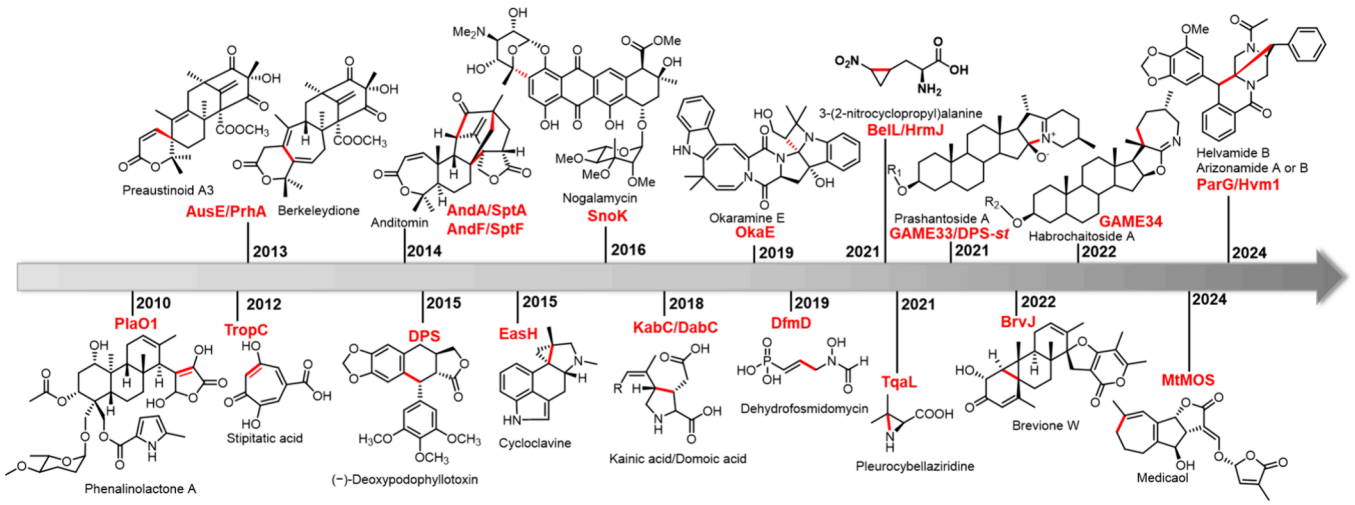

Figure 2. Timeline of the discovery of C−C and C−N bond forming Fe/2OG enzymes and corresponding natural product structures. The red lines represent the newly formed bonds.

https://doi.org/10.1021/acsbiomedchemau.5c00001
ACS Bio Med Chem Au 2025, 5, 238−261

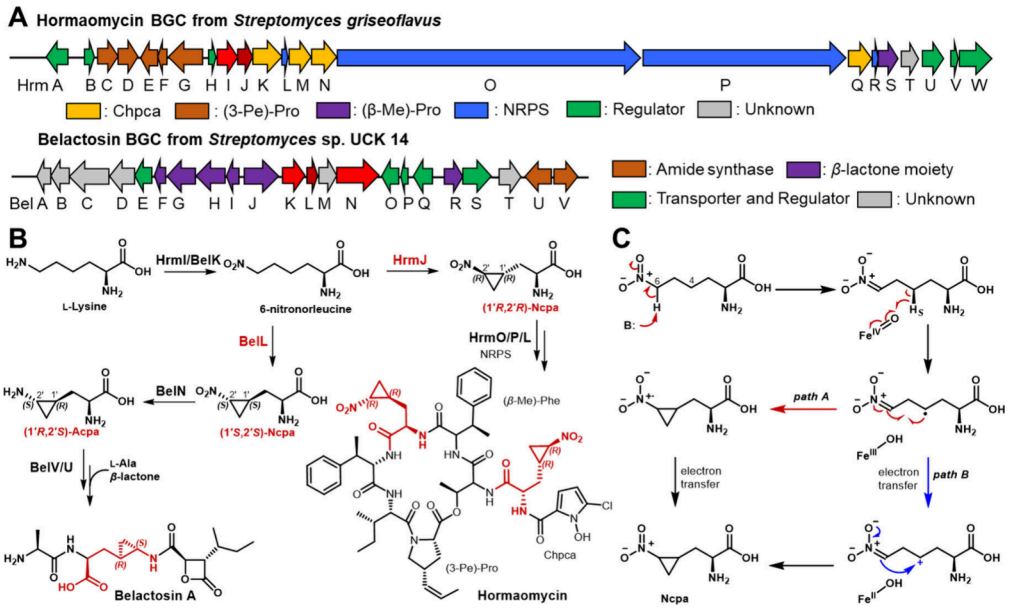

Figure 3. Biosynthetic gene clusters (A) and corresponding biosynthetic pathways (B) of belactosin and hormaomycin. (C) Possible mechanisms accounting for cyclopropanation.

Despite the diverse reaction outcomes, chemistry similar to that of canonical hydroxylation nevertheless appears to be involved. Briefly, following the hydrogen atom abstraction, the substrate radical may then undergo radical addition to an electron donor in the form of a π-system or nitrogen with a nonbonding electron pair, resulting in C−C or C−N bond formation. However, a number of studies have also provided evidence for the involvement of a carbocation intermediate such that C−C or C−N bond formation takes place via nucleophilic addition following electron transfer from the substrate radical to the hydroxy−ferric complex. The following sections are devoted to provide detailed examples of these novel chemistries and are organized according to the overall reaction types catalyzed including cyclopropanation, intramolecular cross-linking, oxidative rearrangement, and aziridination. In each section, the biosynthetic pathways and current understanding of how Fe/2OG enzymes catalyze selective reaction types are discussed.

3. CYCLOPROPANATION

The strained three-membered cyclopropyl group is a well-known pharmacophore in several natural products.[59] To date, a number of Fe/2OG enzymes have been identified that catalyze cyclopropanation reactions via different mechanisms.[60] For example, cyclopropanation in the biosynthesis of the indole alkaloid cycloclavine[46] and the meroditerpenoid brevione W[55] starts with a ring contraction, whereas *de novo* biosynthesis of 3-(2-nitrocyclopropyl)alanine (Ncpa) uses a nitro group to initiate cyclopropanation.[53,54] While different strategies are deployed to enable cyclopropanation, an assistant group, e.g., the C═C, C═N, or C═O moiety that is appended on the substrate or generated *in situ*, is involved to compete with the oxygen rebound pathway. Whether a radical or a cation is used to trigger cyclopropanation remains to be established and could be different in each system.

3.1. BelL and HrmJ in Belactosin and Hormaomycin Biosynthesis

Hormaomycin is a depsipeptide isolated from *Streptomyces griseoflavus* W-384.[61,62] The structure of hormaomycin contains a couple of unusual building blocks, including 3-propenylproline ((3-Pe)-Pro), 5-chloro-1-hydroxypyrrole-2-carboxylic acid (Chpca), and 1′*R*,2′*R*-Ncpa (Figure 3B). Belactosins are isolated from *Streptomyces* sp. UCK 14 and characterized by a β-lactone moiety linked to a (1′*R*,2′*S*)-3-(2-aminocyclopropyl)alanine (1′*R*,2′*S*-Acpa) via an amide bond.[63] The Acpa and Ncpa components share very similar structures, with the only differences being the oxidation state of the nitrogen atom and stereochemical configuration of the cyclopropane ring.

Distinctive biosynthetic pathways are utilized to construct belactosin A and hormaomycin (Figure 3A). The backbone skeleton of belactosin A is assembled by ATP-dependent amide synthases (BelV and U),[64,65] whereas the depsipeptide skeleton in hormaomycin is constructed by the nonribosomal peptide synthase (NRPS) assembly line (HrmO, P, and L).[66] Several enzymes are required to construct the precursors to hormaomycin biosynthesis. Formation of Chpca is proposed to begin with the linkage of L-proline with the peptidyl carrier protein HrmL catalyzed by the acyl-CoA synthetase HrmK. Subsequent aromatization catalyzed by two acyl-CoA dehydrogenases HrmM and HrmN, chlorination catalyzed by the halogenase HrmQ,[67] and *N*-hydroxylation by an unknown oxygenase result in the biosynthesis of Chpca. The (3-Pe)-Pro component is derived from L-Tyr following a pathway similar to that of lincomycin biosynthesis.[68] This pathway is mediated by the L-tyrosine hydroxylase HrmE, extradiol dioxygenase HrmF, SAM-dependent methyltransferase HrmC, F_{420}-dependent oxidoreductase HrmD, and γ-glutamyl transpeptidase HrmG. The (β-Me)-Phe is proposed to be derived from α-keto acid phenyllactate processed through a SAM-dependent methyltransferase HrmS and an unknown transaminase.[66] For belactosin A, the β-lactone moiety is built from 2-keto-3-

https://doi.org/10.1021/acsbiomedchemau.5c00001
ACS Bio Med Chem Au 2025, 5, 238−261

methylvalerate[64] by an ATP-dependent enzyme BelH, the cryptic methyltransferase BelI, and a demethylase BelR.[65,69]

Formation of the cyclopropyl precursors 1′*R*,2′*S*-Acpa and 1′*R*,2′*R*-Ncpa involves very similar pathways which include both a heme oxygenase-like dinuclear iron enzyme (HrmI or BelK) and an Fe/2OG enzyme (HrmJ or BelL) (Figure 3B).[53,54,70,71] HrmI/BelK catalyzes the oxidation of L-lysine to L-6-nitronorleucine, which is followed by Fe/2OG enzyme HrmJ/BelL catalyzed cyclopropanation to afford Ncpa. The stereochemical configuration of the Ncpa intermediate is thus highly dependent on the specific enzyme homologue involved. A molybdopterin-dependent enzyme BelN further catalyzes the reduction of 1′*S*,2′*S*-Ncpa to 1′*R*,2′*S*-Acpa in the biosynthetic pathway of belactosins.[70]

Possible mechanisms for cyclopropanation have been investigated by the Abe, Guo, and Chang groups (Figure 3C). Monitoring the decay kinetics of the Fe^{IV}=O complex using stopped-flow optical absorption spectroscopy resulted in measurement of a deuterium-kinetic isotope effect (D-KIE, ca. 12, on the decay rate of the Fe^{IV}=O) when the deuterated isotopologue 4,4-$^2H_2$-L-6-nitronorleucine was used as a substrate. This outcome is indicative of H atom transfer from the C4 position.[72] These results are corroborated by Mössbauer spectroscopy of samples prepared using the freeze–quench technique. The detailed spectroscopic analysis confirmed the generation of Fe^{IV}=O species prior to H atom abstraction from the C4 position.[72]

This led to the hypothesis that the C4 radical once generated undergoes intramolecular radical addition to the nitro enolate (a.k.a. nitronate) at C6.[72] Following C–C bond formation, an electron transfer occurs to complete cyclopropanation (pathway A). However, an alternative mechanistic pathway can be envisioned that involves initial electron transfer to yield a carbocation at C4, followed by nucleophilic addition by the nitro enolate (pathway B). Significant formation of the nitro enolate tautomer is established by analysis of the ^{13}C NMR spectrum. Specifically, 6-^{13}C-L-6-nitronorleucine is found to exhibit two C6 carbon resonances depending on pH which is consistent with equilibration of the nitro and enolate forms.[54] Stereoselective transfer of the C4 *pro-S* H atom is established in the catalytic cycles of HrmJ and BelL using stereoselectively labeled deuterated substrates.[53] Therefore, C–C bond formation at C4 proceeds antarafacially and suprafacially with respect to H atom abstraction in the reactions catalyzed by BelL and HrmJ, respectively.

The variation in the stereoselectivity of cyclopropanation among BelL and HrmJ homologues features their reaction outcomes that are distinct from those of hydroxylases and chlorinases. Instead of oxygen or chloride rebound, a C–C bond formation occurs to furnish cyclopropane ring installation. Several HrmJ homologues from two different bacterial phyla (i.e., *Actinomycetota* and *Proteobacteria*) have also been shown to catalyze the cyclopropanation of 6-nitronorleucine but instead yielding *cis*-cyclopropane as opposed to *trans*-cyclopropane rings. SrBelL and ScBelL produce (1′*S*,2′*R*)-Ncpa and (1′*R*,2′*S*)-Ncpa as the major products, respectively.[72] While HrmJ homologues that catalyze stereoselective cyclopropanation reactions to produce all four product isomers have thus been identified and characterized, the mechanistic features that control the stereochemical outcome of these reactions remain to be established.

3.2. EasH in Cycloclavine Biosynthesis

Cycloclavine is a cyclopropane-containing ergot alkaloid.[73] Cycloclavine was first discovered from the seeds of the plant *Ipomoea hildebrandtii vatke* in 1969 and later isolated from *Aspergillus japonicus* in 1982 (Figure 4).[74,75]

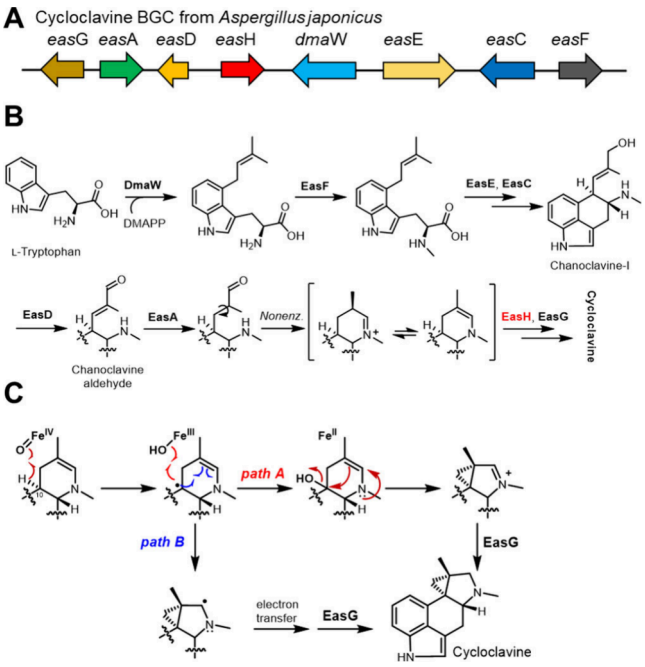

Figure 4. (A) Biosynthetic gene cluster and (B) the proposed biosynthetic pathway of cycloclavine. (C) Possible mechanisms of the EasH-catalyzed cycloproponation.

The biosynthetic gene cluster of cycloclavine was identified by the O'Connor group in 2015 and shown to encode eight proteins. Seven are homologous to previously reported proteins in the biosynthesis of the ergot alkaloids festuclavine and agroclavine (Figure 4A and B).[46] Therefore, cycloclavine shares the biosynthetic intermediate chanoclavine aldehyde with other ergot alkaloids.[73] Its formation involves five enzymes, with L-tryptophan serving as the initial biosynthetic precursor. The prenyltransferase DmaW and *N*-methyl transferase EasF catalyze dimethylallylation and methylation at the benzene ring and α-amino group, respectively. The putative oxidoreductase EasE and catalase EasC mediate intramolecular decarboxylative cyclization to install a cyclohexane, thereby forming chanoclavine-I, which is then oxidized in a reaction catalyzed by EasD to the form chanoclavine aldehyde. The flavin-containing enzyme EasA has been proposed to generate a cyclic iminium intermediate, which is isomerized to a neutral enamine. EasH then triggers C–C bond formation to complete the 3,5-bicyclic ring formation. Final reduction to form cycloclavine is then proposed to be catalyzed by the NADPH-dependent reductase EasG.[46]

As one of the early examples of an Fe/2OG enzyme that catalyzes the biosynthesis of a cyclopropyl ring via C–C bond formation, EasH broadens the reaction scope of this enzyme family. Two mechanisms for cyclopropanation have been proposed (Figure 4C).[76] In the first mechanism, EasH acts as a hydroxylase, leading to C10 hydroxylation such that the newly installed hydroxyl group functions as a leaving group to trigger intramolecular C–C bond formation (pathway A). However,

https://doi.org/10.1021/acsbiomedchemau.5c00001
ACS Bio Med Chem Au 2025, 5, 238–261

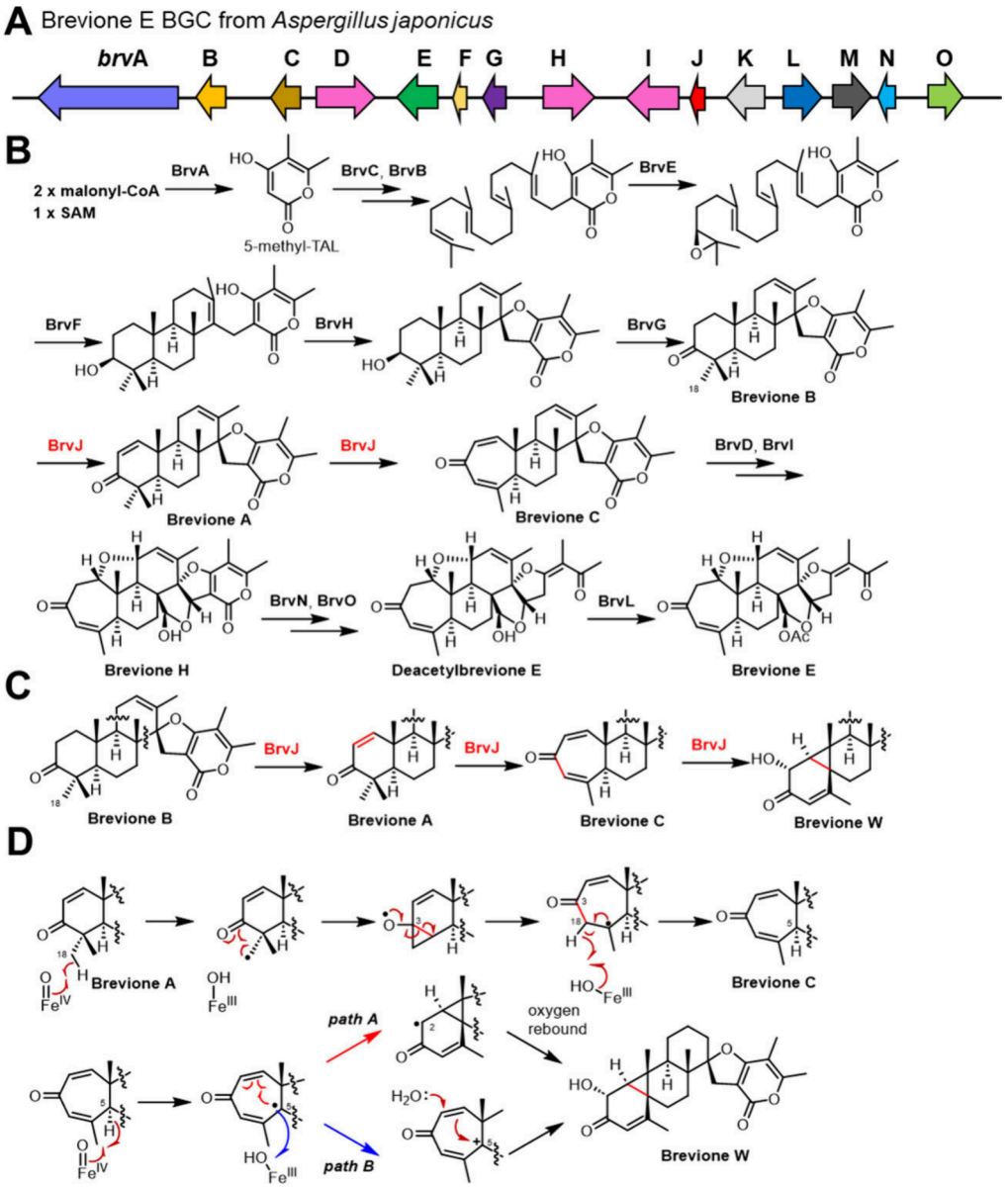

Figure 5. (A) Biosynthetic gene cluster and (B) corresponding biosynthetic pathway of brevione E. (C) Under *in vitro* conditions, BrvJ catalyzes multiple reactions. (D) Possible mechanisms of BrvJ catalyzed oxidative rearrangements.

the crystal structure of EasH bound with 2OG (PDB: 5DAP)[76] revealed that the substrate-binding pocket is hydrophobic and does not contain any potential proton donors in order to protonate and thus stabilize the hydroxyl leaving group. This led to an alternative mechanism involving radical-mediated cyclization (pathway B). Following H atom abstraction from C10, the resulting substrate radical may undergo radical addition to the enamine, thereby forming the cyclopropane and a secondary radical stabilized via conjugation with the tertiary amine before electron transfer completes the reaction. While this reaction could instead proceed via nucleophilic addition of the enamine following one-electron oxidation of the radical intermediate to a tertiary carbocation, computational studies favor radical-mediated cyclization without intermediary carbocation formation.[77]

3.3. BrvJ in Brevione Biosynthesis

Brevione E is a fungal-derived hexacyclic meroterpenoid allelopathic agent isolated from *Penicillium brevicompactum*.[78] The structure of brevione E is initially proposed to include an oxepane,[78] which is later revised to a tetrahydrofuran ring by the Matsuda group (Figure 5B).[55] The same research group revealed that the biosynthetic gene cluster of brevione E in *Penicillium bialowiezense* CBS 227.28 encodes a total of 15 proteins including seven enzymes shared with the setosusin pathway (BrvA−C and BrvE−H) responsible for synthesizing the intermediate brevione B.[79]

Biosynthesis of brevione E begins with formation of 5-methyl triacetic acid lactone (5-methyl-TAL) catalyzed by the nonreducing polyketide synthase BrvA before geranylgeranylation, which is mediated by the prenyltransferase BrvB using geranylgeranyl pyrophosphate (GGPP) provided by the GGPP synthase BrvC. Subsequently, a flavin-dependent monooxygenase BrvE catalyzes epoxidation of the olefin, and the resulting product is cyclized by the terpene cyclase BrvF. The P450 enzyme BrvH then catalyzes spiro ring formation, which is followed by oxidation catalyzed by the short-chain dehydro-

https://doi.org/10.1021/acsbiomedchemau.5c00001
ACS Bio Med Chem Au 2025, 5, 238−261

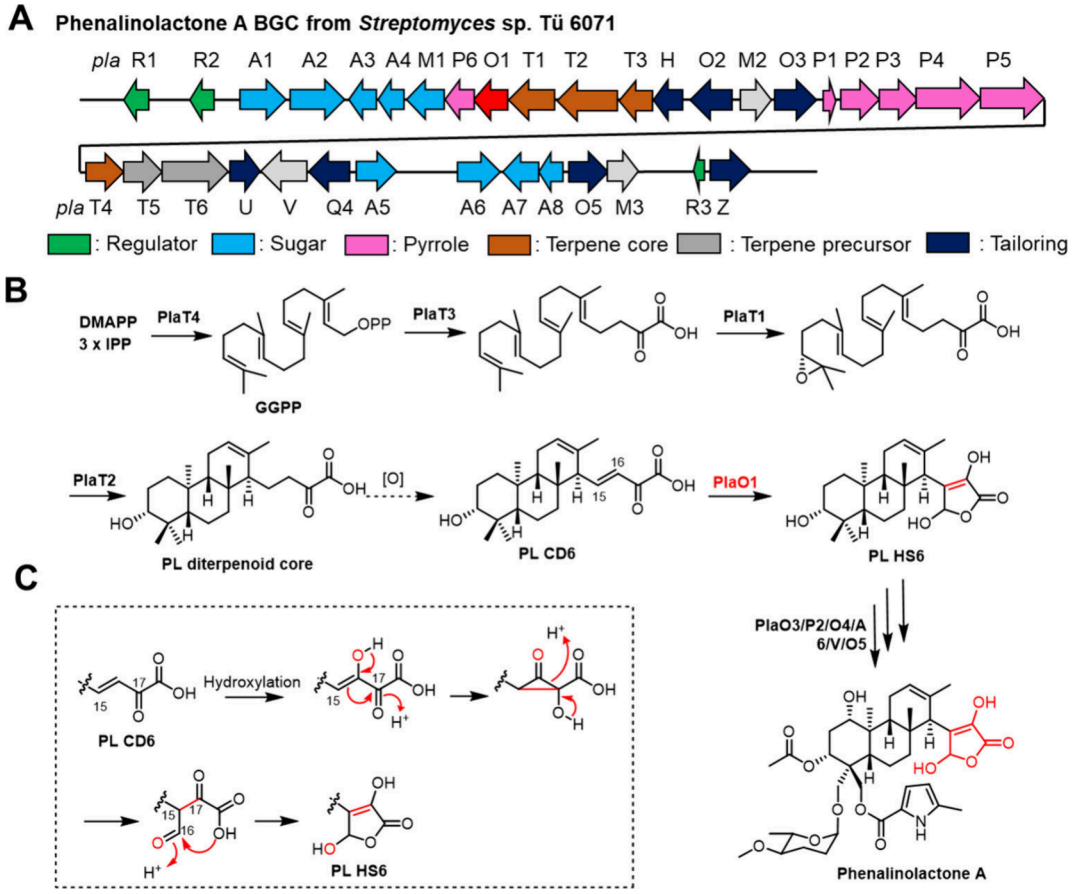

Figure 6. (A) Biosynthetic gene cluster and (B) corresponding biosynthetic pathway of phenalinolactone A. (C) The plausible mechanism for γ-butyrolactone formation catalyzed by PlaO1.

genase BrvG to yield brevione B. Heterologous expression experiments established that Fe/2OG enzyme BrvJ plays a vital role in converting brevione B into brevione C via brevione A as a potential intermediate.[55] Feeding experiments using sodium 1,2-$^{13}C_2$-acetate and a strain producing brevione A and C indicated the ring expansion occurs at C18.[55] Two P450 enzymes BrvD and BrvI then catalyze multiple oxidative reactions to form brevione H. BrvN subsequently hydrolyzes the pyrone moiety of brevione H, and a SAM-dependent decarboxylase BrvO performs decarboxylation to yield deacetylbrevione E, which is *O*-acetylated by BrvL to produce brevione E.

As an Fe/2OG enzyme, BrvJ can catalyze three successive oxidation reactions including the desaturation, ring expansion, and cyclopropanation to afford brevione W. Cyclopropanation, however, has only been observed under *in vitro* conditions (Figure 5C). Biochemical assays established that brevione A and C are intermediates in the production of brevione W, leading to the proposed reaction mechanism shown in Figure 5D that includes ring expansion and cyclopropanation.[55] The reaction begins with H atom transfer to yield the C18 substrate radical that attacks the C3 carbonyl to form a cyclopropyl ring and an oxygen radical. This is followed by C3−C4 bond homolysis that results in ring expansion before a second H atom transfer from C18 yields brevione C. Oxidation of brevione C to W is then proposed to be initiated by H atom abstraction from C5. The resultant radical triggers cyclopropyl ring formation between C5 and C1 followed by oxygen rebound to yield brevione W; however, another pathway including a carbocation intermediate has also been proposed.[55] Interestingly, BrvJ is homologous to SetK that utilizes brevione B as substrate for hydroxylation in setosusin biosynthesis.[79] Comparison of predicted substrate-binding sites from model structures of BrvJ and SetK combined with mutagenesis have led to the conversion of BrvJ to a hydroxylase.[55]

3.4. PlaO1 in Phenalinolactone A Biosynthesis

Phenalinolactone A is a diterpenoid glycoside antibiotic isolated from *Streptomyces* sp. Tü 6071.[80−82] Its structure contains the core *anti*/*anti*/*syn*-perhydrophenanthrene decorated with a distinct γ-butyrolactone moiety (Figure 6B). The biosynthetic gene cluster of phenalinolactone A (*pla* BGC) has been enclosed by *in situ* gene disruption and heterologous expression experiments (Figure 6A).[83,84]

The biosynthesis of the tricyclic diterpenoid core in phenalinolactone A is elucidated by heterologous reconstitution.[85] PlaT3 adds a three-carbon α-keto acid of unknown origin to GGPP. Sequential epoxidation and cyclization, directed by flavin-dependent monooxygenase PlaT1 and type II terpene cyclase PlaT2, generate the diterpenoid core. A desaturation catalyzed by the unknown enzyme leads to the formation of intermediate PL CD6. After that, an Fe/2OG enzyme PlaO1 catalyzes γ-butyrolactone moiety formation.[39] During PlaO1 reaction, following hydroxylation, a three-membered intermediate is proposed to be generated that undergoes ring-opening and cyclization to afford butyrolactone (PL HS6, Figure 6C). Finally, after multistep structural modifications, including three hydroxylations by three P450s

https://doi.org/10.1021/acsbiomedchemau.5c00001
ACS Bio Med Chem Au 2025, 5, 238−261

PlaO3/O4/O5 and addition of acetyl, 5-methylpyrrole-2-carboxylic acid, and L-amicetose moieties, presumably catalyzed by acyltransferase PlaV/P2 and glycosyltransferase PlaA6, phenalinolactone A is furnished.[39]

4. RING FORMATION

4.1. KabC and DabC in Kainic Acid and Domoic Acid Biosynthesis

Domoic acid and kainic acid are glutamate receptor agonists[86−88] which have been isolated from the red macroalgae *Chondria armata* and *Digenea simplex*,[89] respectively. Their structures have a common scaffold derived from glutamate and a pyrrolidine isoprenoid (Figure 7B−C).

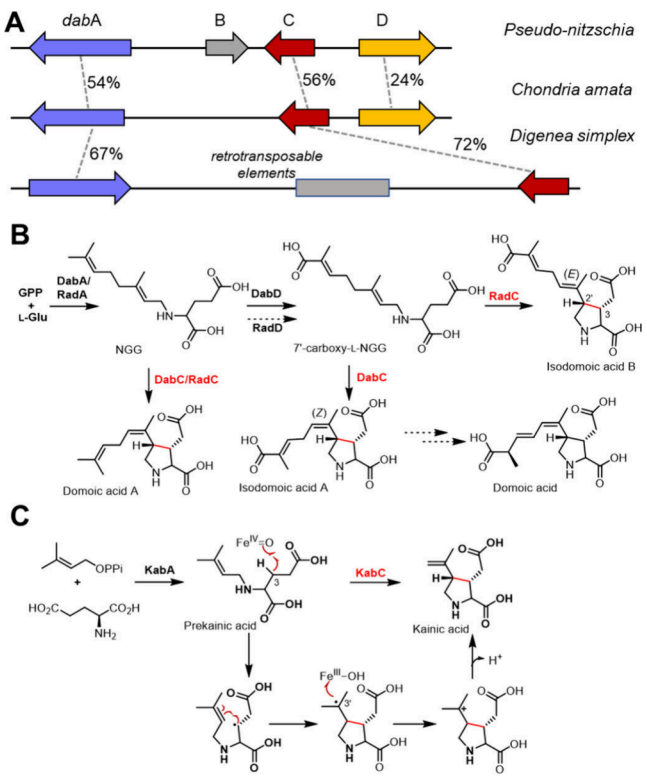

Figure 7. (A) Biosynthetic gene clusters and biosynthetic pathways of (B) domoic acid and (C) kainic acid. Possible mechanisms for pyrrolidine formation are shown in panel C.

Feeding experiments demonstrated that domoic acid arises from the condensation of glutamic acid and geranyl pyrophosphate (GPP).[90,91] The biosynthetic gene cluster of domoic acid (*dab*) is biochemically investigated from the *Pseudonitzschia multiseries* and found to encode three functional proteins. The *N*-prenyltransferase DabA catalyzes condensation between GPP and L-Glu to yield *N*-geranyl-L-glutamic acid (NGG) followed by the P450 enzyme DabD that catalyzes oxidation of NGG to 7′-carboxy-NGG. The Fe/2OG enzyme DabC mediates oxidative cyclization of 7′-carboxy-L-NGG to yield isodomoic acid A (Figure 7B).[49] The isomerase that converts isodomoic acid A to domoic acid remains to be identified.

A homologous gene cluster of *dab*BGC from the first reported domoic acid producing strain *Chondria armata* (*rad*) is also reported (Figure 7A).[92] Notably, the DabB, a hypothetical protein, homologue is missing in *rad*, and RadC catalyzes 7′-carboxy-L-NGG to isodomoic acid B as the major product rather than isodomoic acid A, which are *E*/*Z*-isomers of one another.[92] Additionally, RadC is found to accept NGG as a preferred substrate and furnish domoic acid A formation.[93] The biosynthesis of kainic acid is directed by the *kab* gene cluster from *Digenea simplex*, which encodes a concise two-enzyme biosynthetic pathway. KabA catalyzes condensation of L-Glu and dimethylallyl pyrophosphate (DMAPP), which is followed by KabC catalyzed cyclization.[48]

The mechanism of pyrrolidine formation catalyzed by KabC has been investigated using pre-steady state kinetics and freeze−quench coupled Mössbauer spectroscopy.[94] A primary deuterium KIE is thus measured for the decay of the Fe^{IV}=O intermediate using C3-deuterated prekainic acid as the substrate, indicating that C3 is the site of initial H atom abstraction. Furthermore, the reaction outcome could be redirected to hydroxylation at C3′ via the oxygen rebound upon successive fluorination of a terminal methyl group suggesting involvement of a carbocation intermediate in the desaturation step.[94] The overall reaction has thus been proposed to begin with transfer of the C3 H atom to the Fe^{IV}=O complex to produce a C3 substrate radical that undergoes radical addition to the olefin moiety, leading to pyrrolidine ring formation. Subsequent electron transfer and proton transfer from the methyl group lead to desaturation that furnishes kainic acid.

4.2. DPS in (−)-Deoxypodophyllotoxin Biosynthesis

Podophyllotoxin is an aryltetralin-type lignan discovered in the plant *Podophyllum peltatum* in 1881, and its chemical structure has been later solved in 1932.[95] Podophyllotoxin features a tetracyclic fused system (A−D rings) with a pendant benzene ring (E ring) (Figure 8A).[96−98] Biosynthesis of podophyllotoxin begins with coniferyl alcohol derived from the phenylpropanoid pathway.[98] Dimerization catalyzed by dirigent protein oxidase (DPO) and dirigent protein (DIR) converts

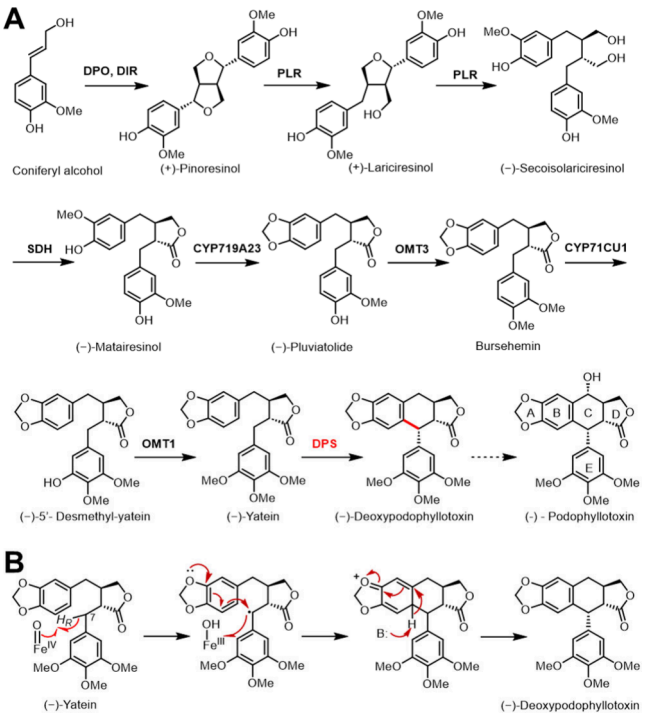

Figure 8. (A) Proposed biosynthetic pathway of (−)-deoxypodophyllotoxin. (B) Possible mechanism of DPS-catalyzed ring closure.

https://doi.org/10.1021/acsbiomedchemau.5c00001
ACS Bio Med Chem Au 2025, 5, 238−261

coniferyl alcohol to (+)-pinoresinol.[99] Afterward, a pinoresinol-lariciresinol reductase (PLR) converts (+)-pinoresinol into (−)-secoisolariciresinol via (+)-lariciresinol.[100] Oxidation of (−)-secoisolariciresinol is then catalyzed by a NAD-dependent secoisolariciresinol dehydrogenase (SDH) to form (−)-matairesinol.[101] The methylenedioxy bridge of (−)-pluviatolide is constructed by the P450 enzyme CYP719A23.[102] However, it is not until 2015 that Sattely's group discovered the biosynthesis of (−)-deoxypodophyllotoxin.[45] Formation of (−)-deoxypodophyllotoxin from (−)-pluviatolide requires four enzymes, including one P450 enzyme (CYP71CU1) for hydroxylation, two *O*-methyltransferases, OMT1 and OMT3, for methylation, and one Fe/2OG enzyme (DPS) for the ring C installation. Notably, the hydroxylase needed to convert (−)-deoxypodophyllotoxin to podophyllotoxin remains unknown.

Deoxypodophyllotoxin synthase (DPS) catalyzes C−C bond formation to yield the six-membered C ring of the fused tetracyclic system. While DPS catalyzed Csp^2−Csp^3 bond formation is similar to other types of C−C bond formation enabled by Fe/2OG enzymes, in this instance, the π-system is part of an aromatic ring. A possible reaction mechanism for DPS has been proposed based on substrate-bound protein structures, biochemical assays of substrate analogs that replace the *para*-methoxy group on the pendant benzene ring with other moieties (e.g., H and CH_3) and studies of model chemical reactions (Figure 8B).[103−105] The reaction is thus hypothesized to proceed through carbocation-triggered C−C bond formation in which the *para*-substituent significantly affects the reaction efficiency. An electron-donating group stabilizes the carbocation, thus facilitating C−C bond formation. In the presence of an electron-withdrawing group, however, hydroxylation is observed as a side reaction. The crystal structure of the DPS•Fe•succinate•(±)-yatein complex (PDB: 7E38)[104] reveals that the substrate binds in a U-shaped conformation in the active site, which facilitates H atom abstraction from C7 to form the initial substrate radical. The structure also reveals tight anchoring of the D and E rings that explains the observed stereoselectivity of C ring formation.[105] Recent computational studies have implied an unusual radical reaction mechanism that includes the participation of CO_2,[106,107] the byproduct generated from the oxidative decarboxylation of 2OG. However, experimental evidence of this proposal is still needed.

4.3. OkaE in Okaramines Biosynthesis

Okaramines are a class of insecticidal fungal indole alkaloids isolated from *Penicillium simplicissimum* and *Aspergillus aculeatus*.[108−113] Okaramines are characterized by the eight-membered azocine ring; however, okaramines such as B−E also contain a unique four-membered azetidine ring (Figure 9B). Structure−activity relationship studies have demonstrated that both the azetidine and azocine rings are indispensable for insecticidal activity.[114]

The biosynthetic gene cluster for okaramines (*oka*) is reported by the Lin group (Figure 9A).[50] The *oka* gene cluster only encodes seven functional enzymes required for the biosynthesis of these structurally complex natural products.[115] Two of the gene products are responsible for production of the prenylated diketopiperazine (DKP), diprenyl cyclo-L-Trp-L-Trp (Figure 9B). OkaA is a NRPS enzyme that catalyzes formation of the DKP skeleton, and a dimethylallyltryptophan synthase (DMATS) OkaC enables reverse prenylation at N1

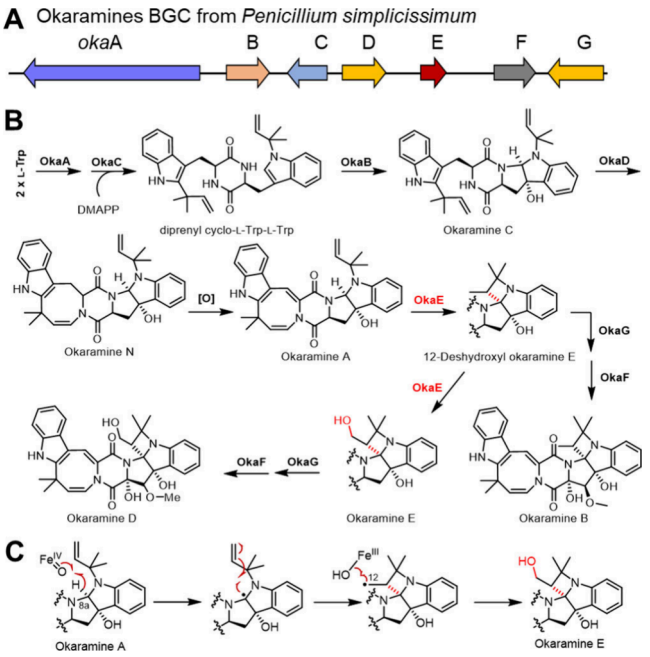

Figure 9. Biosynthesis of okaramines. (A) Biosynthetic gene cluster of okaramines. (B) The proposed biosynthetic pathway of okaramines. (C) The proposed mechanism of OkaE-catalyzed azetidination.

and C2′ of the indole ring. This biosynthesis is followed by an epoxidation and cyclization catalyzed by the flavin-dependent monooxygenase OkaB to afford hexahydropyrrolo[2,3-*b*]indole in Okaramine C. OkaD is a P450 enzyme that catalyzes the introduction of the eight-membered azocine ring via C−N bond formation to yield okaramine A. Of particular interest is the Fe/2OG enzyme OkaE that mediates formation of the four-membered azetidine. This core skeleton is further decorated with okaramine B and D through hydroxylation and methylation by the P450 enzyme OkaG and the methyltransferase OkaF.

A possible reaction mechanism has been proposed for the four-membered azetidine (Figure 9C).[50] Following H atom abstraction from C8a, the substrate radical adds to the olefin moiety to form the azetidine and C12 radical. Oxygen rebound leads to okaramine E. Notably, the *in vitro* assay revealed that OkaE converts okaramine A into 12-deshydroxyl okaramine E, without hydroxylation, if the reaction buffer contains a very high concentration of reductant such as 20 mM β-mercaptoethanol, which implies that the product radical can be quenched by reducing species. The 12-deshydroxyl okaramine E can be further hydroxylated in the presence of OkaE to yield okaramine E (Figure 9B).

4.4. SnoK in Nogalamycin Biosynthesis

Nogalamycin is a type II polyketide anthracycline produced by *Streptomyces nogalater*.[116−118] The structure of nogalamycin is distinct from those of other anthracyclines because it contains two deoxysugars. L-Nogalamine is attached to polyketide aglycone via two bonds, the *O*-glycosylation at C1 and a C−C bond between C2 and C5″, whereas nogalose is attached at the C7 position (Figure 10B).

The nogalamycin biosynthetic gene cluster (*sno*) spans approximately 38 kb length in the genome of *S. nogalater* (Figure 10A).[119−125] Biosynthesis of nogalamycin can be divided into two stages: formation of the anthracycline aglycone and subsequent modification via glycosylation

https://doi.org/10.1021/acsbiomedchemau.5c00001
ACS Bio Med Chem Au 2025, 5, 238−261

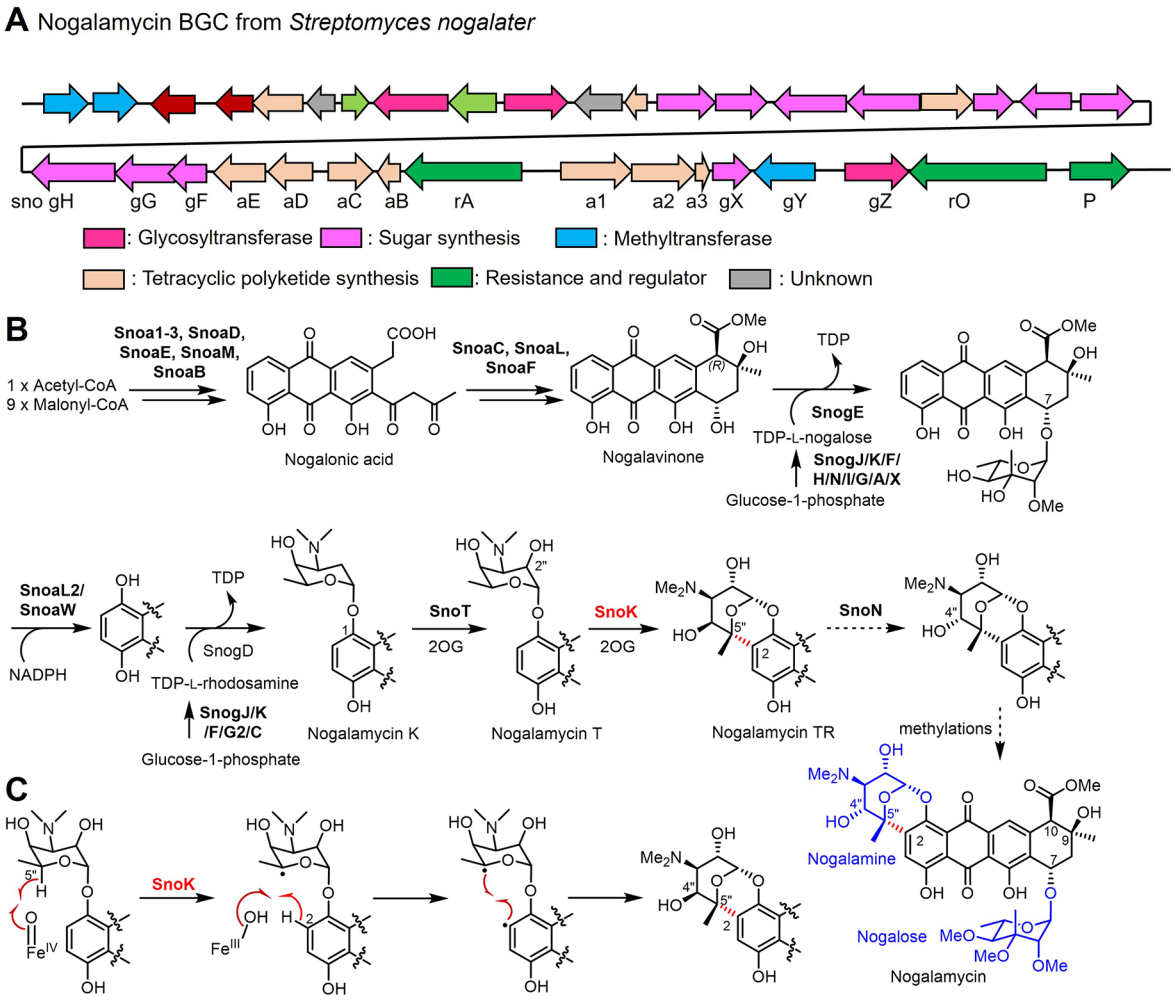

Figure 10. Biosynthesis of nogalamycin. (A) Biosynthetic gene cluster and (B) proposed biosynthetic pathway of nogalamycin. (C) The proposed mechanism of SnoK-catalyzed C−C bond formation.

(Figure 10B).[125,126] Aglycone is derived from one acetyl-CoA and nine malonyl-CoA, which are assembled in nine rounds of iterative Claisen condensations catalyzed by minimal polyketide synthase. The resulting linear decaketide is converted to tricyclic nogalonic acid in a series of enzyme catalyzed reactions. Subsequent methylation, cyclization, and ketoreduction yield the tetracyclic anthracycline scaffold of nogalavinone. The tailoring steps begin with glycosylation at C7 catalyzed by SnogE. After hydroxylation catalyzed by a two-component monooxygenase SnoaW/SnoaL2,[127] SnogD catalyzes *O*-glycosylation at C1 with another deoxysugar, L-rhodosamine.[127] The Rieske enzyme SnoT catalyzes 2″-hydroxylation of L-rhodosamine after the initial glycosylation step.[128] In 2016, the Metsä-Ketelä group revealed that this is followed by an unusual C5″−C2 carbocyclization catalyzed by the Fe/2OG enzyme SnoK upon *in vitro* assay of nogalamycin K as the substrate;[47] however, later works indicated that nogalamycin T is likely the native substrate for SnoK.[128] In the same work, SnoN is found to catalyze epimerization at C4″.[47] It is possible that the remaining methyltransferases (Sno gM, gL, and gY) catalyze the final series of *O*-methylation reactions on nogalose to generate nogalamycin.

Based on the proximity of both carbons to the iron center in the crystal structure of Fe•2OG•SnoK docked with the substrate nogalamycin K, a radical mechanism for C5″−C2 cyclization has been proposed (Figure 10C). The reaction is initiated by H atom abstraction from C5″. A second H atom transfer from C2 to the Fe^{III}−OH followed by radical recombination forms the C5″−C2 bond. More expreimts will be needed toestablish the reaction mechanism. It is noteworthy that SnoK is structurally similar to epimerase SnoN with an overall RMSD value of 0.83 Å. Furthermore, swapping amino acids in the active site allows switching reaction outcomes.[129]

4.5. ParG and Hvm1 in Piperazine Biosynthesis

Piperazine contains a six-membered heterocycle with two nitrogen atoms at opposite positions.[130] A diverse array of phenylpropanoid piperazines have been discovered from fungi. The main structural features of them are a central piperazine ring with different substituents at both of nitrogen atoms as well as complex ring formation.[130] Recently, two Fe/2OG enzymes Hvm1 and ParG are identified to catalyze these modifications in the biosynthesis of helvamide B and arizonamides (Figure 11A and B).[56,57]

Biosynthesis of the piperazine core in helvamide B and arizonamide A involves the monomodular NRPS (ParA/Hvm11) coupled with a NmrA-like reductase (ParB/Hvm10) to generate xenocockiamide H. Similar to the biosynthetic pathway of hancockiamide,[131] methoxy and methylenedioxy groups are proposed to be introduced via the action of four enzymes (tyrosinase ParI/Hvm8, FAD-dependent phenol

https://doi.org/10.1021/acsbiomedchemau.5c00001
ACS Bio Med Chem Au 2025, 5, 238−261

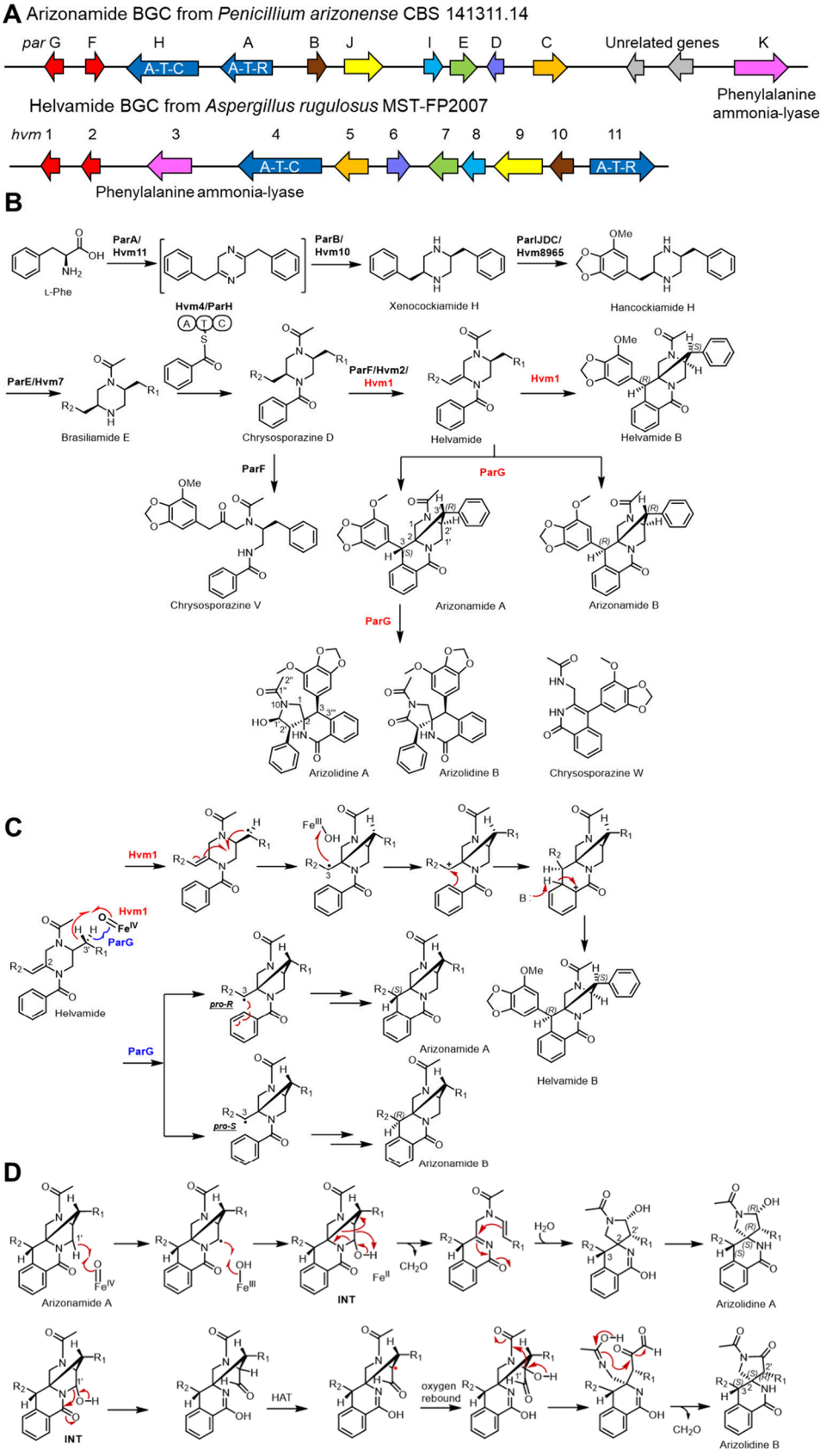

Figure 11. (A) Biosynthetic gene clusters and (B) the proposed biosynthetic pathways of helvamide B and arizonamides. (C) Proposed mechanisms for helvamide B and arizonamides A and B catalyzed by Hvm1 and ParG with helvamide as the substrate. (D) Proposed mechanisms for arizolidines A and B catalyzed by ParG using arizonamide A as the substrate.

https://doi.org/10.1021/acsbiomedchemau.5c00001
ACS Bio Med Chem Au 2025, 5, 238−261

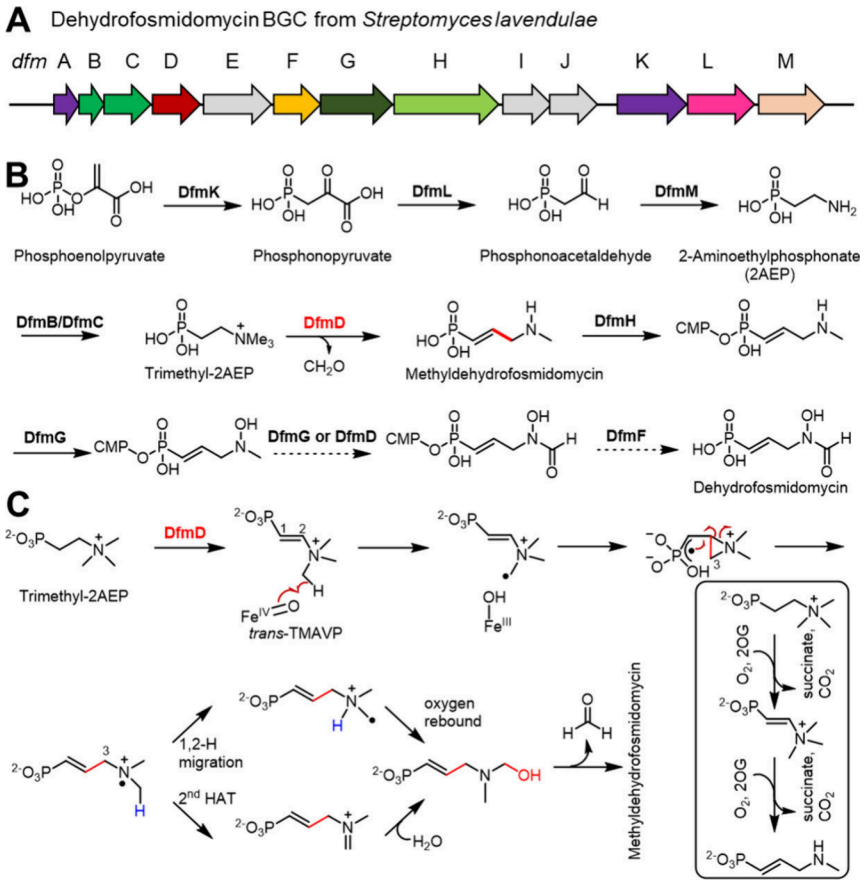

Figure 12. (A) Biosynthetic gene cluster and (B) proposed biosynthetic pathway of dehydrofosmidomycin. (C) Proposed mechanism for DfmD catalyzed desaturation and C−C bond formation.

hydroxylase ParJ/Hvm9, *O*-methyltransferase ParD/Hvm6, and P450 ParC/Hvm5) to yield hancockiamide H.[56,57] Subsequent acetylation and benzoylation of the two amino groups are catalyzed by the acetyltransferase ParE/Hvm7 and the NRPS ParH/Hvm4 to yield chrysosporazine D. Dehydrogenation of chrysosporazine D to helvamide is catalyzed by the Fe/2OG enzyme ParF/Hvm2. ParF has also been reported to catalyze the C2 hydroxylation of chrysosporazine D that results in piperazine cleavage to yield chrysosporazine V.

Helvamide serves as a common substrate for the Fe/2OG enzymes ParG and Hvm1 to generate helvamide B and arizonamides A and B, respectively, via consecutive C−C bond formations. These three compounds are all stereoisomers of one another that differ only in the stereochemistry at C3 and C3′. Hvm1 can catalyze desaturation of chrysosporazine D similar to ParF and Hvm2. Moreover, *in vitro* assays have demonstrated that ParG can further catalyze the transformation of arizonamide A into the spirocyclic arizolidines A and B as well as chrysosporazine W; however, these compounds have not been detected in the metabolic profile of the producing strain (Figure 11B).[56,57]

Hvm1 and ParG catalyzed ring construction involves two consecutive C−C bond formations. Starting from H atom abstraction from the C3′ position, the resulting radical adds to the double bond to form the first C−C bond between C2 and C3′ and a second radical. A carbocation is proposed to trigger a second C−C bond formation followed by rearomatization to furnish helvamide B (Figure 11C).[56] However, the detailed mechanisms remain to be elucidated, and an alternative proposal involves radical addition to the phenyl ring to generate the second C−C bond in arizonamides A and B.[57] Prediction of the ParG structure using AlphaFold2 combined with molecular docking and mutagenesis has implicated Phe67 as a crucial residue in determining the stereochemical course of the second C−C bond formation.[57] In particular, Phe67 may induce a conformational change that positions the radical intermediate for C−C bond formation with *S* versus *R* stereochemistry at C3 of arizonamide A and B, respectively (Figure 11C). Formation of the spirocyclic arizolidines A and B is a consequence of further oxidative rearrangement which appears to be triggered by hydroxylation at C1′ (Figure 11D). Furthermore, arizolidine A cannot be converted into arizolidine B *in vitro*, such that a distinct pathway that includes a second intermediary hydroxylation reaction may underlie its formation.[57] The reactions catalyzed by Hvm1 and ParG are remarkable; elucidation of their mechanisms will require further study.

5. REARRANGEMENT

5.1. DfmD in Dehydrofosmidomycin Biosynthesis

Fosmidomycin (FR-31564) and its unsaturated derivative dehydrofosmidomycin (FR-32863) are discovered from *Streptomyces lavendulae*.[132−134] Although the biogenesis of fosmidomycin remains unknown, the biosynthetic gene cluster (*dfm*) of dehydrofosmidomycin has been identified in *S. lavendulae*, and the biosynthetic pathway is well-characterized through heterologous protein expression, intermediate characterization, and biochemical experiments (Figure 12A and B).[51]

https://doi.org/10.1021/acsbiomedchemau.5c00001
ACS Bio Med Chem Au 2025, 5, 238−261

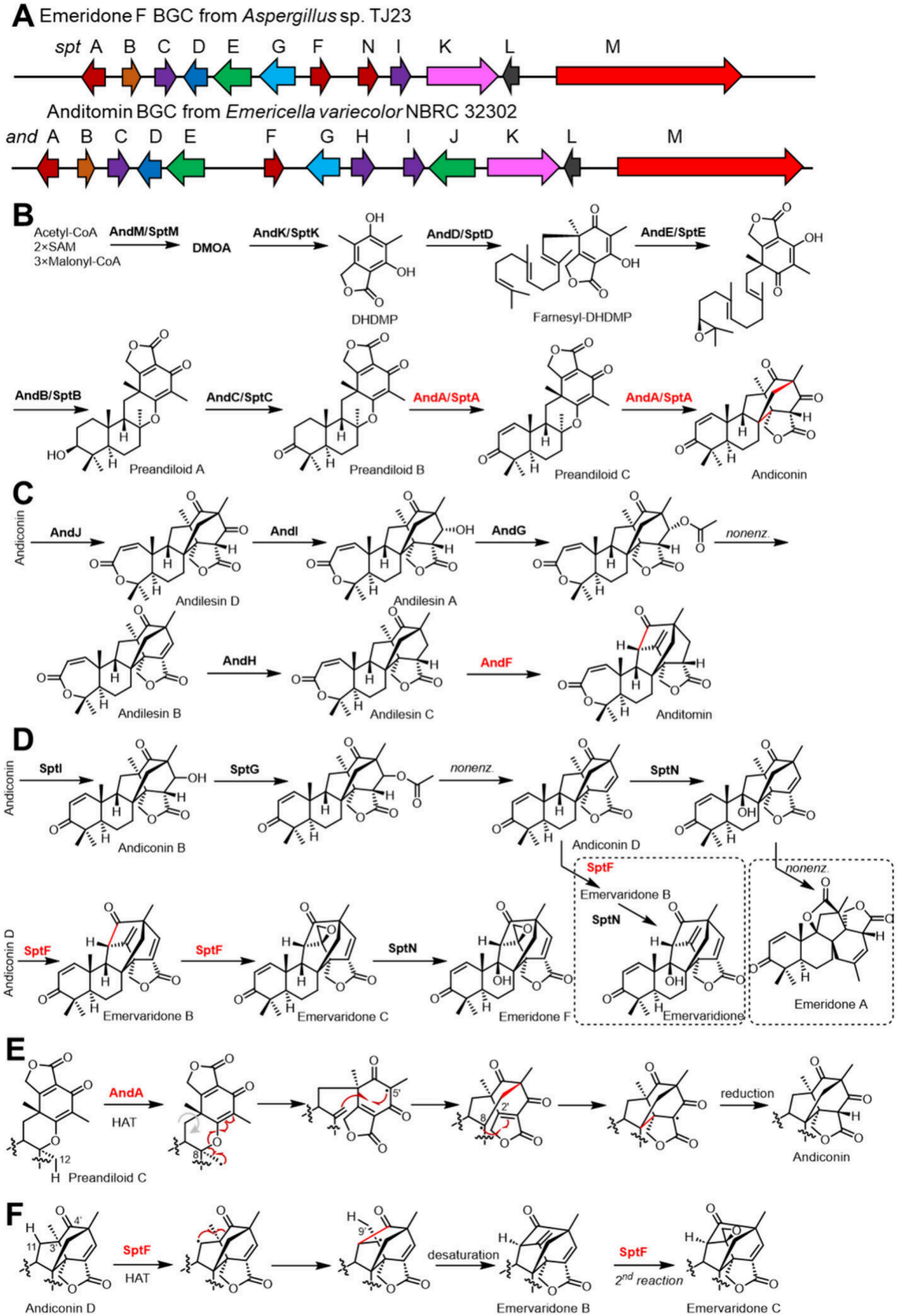

Figure 13. Biosynthesis of anditomin and emeridone F. Biosynthetic gene clusters (A) and proposed biosynthetic pathways of (B) andiconin, (C) anditomin, and (D) emeridone F. Proposed reaction mechanisms for (E) AndA and (F) SptF.

https://doi.org/10.1021/acsbiomedchemau.5c00001
ACS Bio Med Chem Au 2025, 5, 238−261

Biosynthesis of dehydrofosmidomycin thus begins with conversion of phosphoenolpyruvate to phosphonopyruvate catalyzed by PEP mutase (DfmK)[135] followed by transformation to 2-aminoethylphosphonate (2AEP) under the actions of phosphonopyruvate decarboxylase DfmL and aminotransferase DfmM. Subsequently, SAM-dependent methyltransferases DfmB and/or DfmC catalyze the methylations of 2AEP to trimethyl-2AEP which is utilized by an Fe/2OG enzyme DfmD to afford methyldehydrofosmidomycin through a two-step reaction.[51,136,137] After that, the nucleotide transferase DfmH is proposed to catalyze the transfer of a CMP group to methyldehydrofosmidomycin, followed by *N*-hydroxylation catalyzed by a flavin-dependent amine monooxygenase DfmG. The remaining oxidation of the methyl group to a formyl group and the removal of the CMP may be performed by DfmG or DfmD and the metallophosphoesterase DfmF to yield dehydrofosmidomycin.

The reaction mechanism of DfmD has been investigated by the Metcalf, Guo, and Chang groups.[136,137] Because conversion of trimethyl-2AEP to methyldehydrofosmidomycin and formaldehyde is a four-electron oxidation process, it likely involves two turnovers catalyzed by DfmD with an intermediate product. Using ^{13}C-labeled substrate isotoplogues and substoichiometric concentrations of 2OG, the previously uncharacterized desaturated intermediate 2-(trimethylamino)-vinylphosphonate (TMAVP) is identified,[136] thereby confirming that the overall transformation includes sequential desaturation and rearrangement reactions requiring 2 equiv of 2OG for the complete reaction. In addition, incubation of synthetic *trans*-TMAVP with DfmD reaction conditions further proved TMAVP is an intermediate rather than a shunt product.[137] Transient kinetic studies coupled with Mössbauer measurements revealed that the Fe^{IV}═O intermediate in the desaturation reaction is unusually long-lived. Additionally, the quaternary ammonium center of trimethyl-2AEP is found to be critical for desaturation such that dimethyl-2AEP only undergoes hydroxylation.[136]

In order to determine the site of H atom abstraction during the rearrangement reaction, a substrate isotopologue bearing one deuterated methyl and two methyl groups at natural abundance is synthesized for an internal competition experiment.[136] The mass spectrometry results reveal a distribution of product isotopologues with different deuterium incorporated positions, indicating that rearrangement begins with H atom transfer from an *N*-methyl group. The resulting *N*-methyl radical then adds to the double bond introduced during the first half-reaction to generate an *N*,*N*-dimethyl aziridinium cation radical stabilized via conjugation with the phosphonate moiety. Rearrangement and hydroxylation via two proposed pathways result in alkyl chain elongation and demethylation with the elimination of a formaldehyde (Figure 12C).

5.2. AndF and SptF in Anditomin and Emeridone F Biosynthesis

Fungal meroterpenoids derived from 3,5-demethylorsellinic acid (DOMA) and terpenoid represent a class of natural products notable for their structural complexity. Several Fe/2OG enzymes have been found to be responsible for rearrangement reactions during the biosynthesis of anditomin,[43] emeridone F,[138] austinol,[41] and paraherquonin.[42]

Anditomin is first found from *Aspergillus variecolor*.[139] Isotope-feeding studies reveal that it is constructed from DMOA and farnesyl pyrophosphate (FPP).[139−142] More recently, emeridone F[143] and the structurally similar emervaridones[144] are isolated from *Emericella* sp. TJ29. The biosynthetic gene clusters of anditomin (*and* BGC)[43] and emeridone F (*spt* BGC)[138] are nearly the same except that the former encodes a flavin-dependent monooxygenase AndJ for seven-membered lactone synthesis and a short-chain dehydrogenase/reductase AndH for enoyl reduction at the C6′−C7′ position. The *spt* BGC also encodes the Fe/2OG enzyme SptN that catalyzes C9 hydroxylation (Figure 13A).

The biosynthetic pathways of both anditomin and emeridone F have been proposed to include the common intermediate andiconin. Its biosynthesis involves a type-I nonreducing PKSs AndM/SptM that produces DMOA during the initial stages of the pathway. Following hydroxylation and lactonization enabled by the bifunctional P450 AndK/SptK, 5,7-dihydroxy-4,6-dimethylphthalide (DHDMP) is produced. This is followed by sequential reactions catalyzed by a prenyltransferase (AndD/SptD), an epoxidase (AndE/SptE), and a terpene cyclase (AndB/SptB) that produce pentacyclic preandiloid A. Subsequent transformation to preandiloid B is catalyzed by the short chain dehydrogenase/reductase AndC/SptC. The Fe/2OG enzyme AndA then catalyzes formation of the enone preandiloid C, which rearranges to the bicyclo[2.2.2]octane core of andiconin (Figure 13B). Interestingly, *in vitro* experiments reveal that both dehydrogenation and rearrangement are almost completely abolished in the absence of ascorbate.[43]

Andiconin is oxidized to andilesin D via Baeyer−Villiger oxidation catalyzed by AndJ before ketoreduction and acetylation, and nonenzymatic elimination of acetate yields andilesin B. The second SDR AndH catalyzes enoyl reduction to generate andilesin C, which is recognized by the Fe/2OG enzyme AndF to generate anditomin (Figure 13C). In the biosynthesis of emeridone F (Figure 13D), after andiconin D formation via the activities of SptI and SptG, the Fe/2OG enzyme SptF catalyzes oxidative rearrangement to generate emervaridone B. SptF can also catalyze epoxidation of emervaridone B to yield emervaridone C, which is then hydroxylated to produce emeridone F by SptN. Notably, SptN can hydroxylate andiconin D at the C9 position, which induces rearrangement to afford emeridone A.

Based on protein structures, mutagenesis, and computations, the AndA catalyzed rearrangement is proposed to begin with H atom abstraction from the C12 methyl group. The resulting radical induces C−O cleavage that produces the exocyclic double bond and a radical at C5′. The reaction continues through sequential C−C bond formations before the final radical is reduced to yield andiconin (Figure 13E).[44] The biological reductant remains unknown. Structural and mutational experiments reveal that Arg239 and Tyr272 are essential for rearrangement; however, variants at these positions retain dehydrogenation activity.

While AndF and SptF share 94% protein sequence identity, SptF not only catalyzes ring oxidative rearrangement reaction (andiconin D → emervaridone B) but also enables epoxidation to yield emervaridone C (Figure 13F).[138] A mechanism of SptF has been proposed. Following HAT at C11, a radical triggers C4′−C3′ bond cleavage, which is followed by C4′−C11 single bond and C3′−C9′ double bond formations to result in emervaridone B. Finally, a second round of oxidation results in the epoxidation of emervaridone C. SptF is a promiscuous enzyme that accommodates the AndF substrate andilesin C as well.[145]

https://doi.org/10.1021/acsbiomedchemau.5c00001
ACS Bio Med Chem Au 2025, 5, 238−261

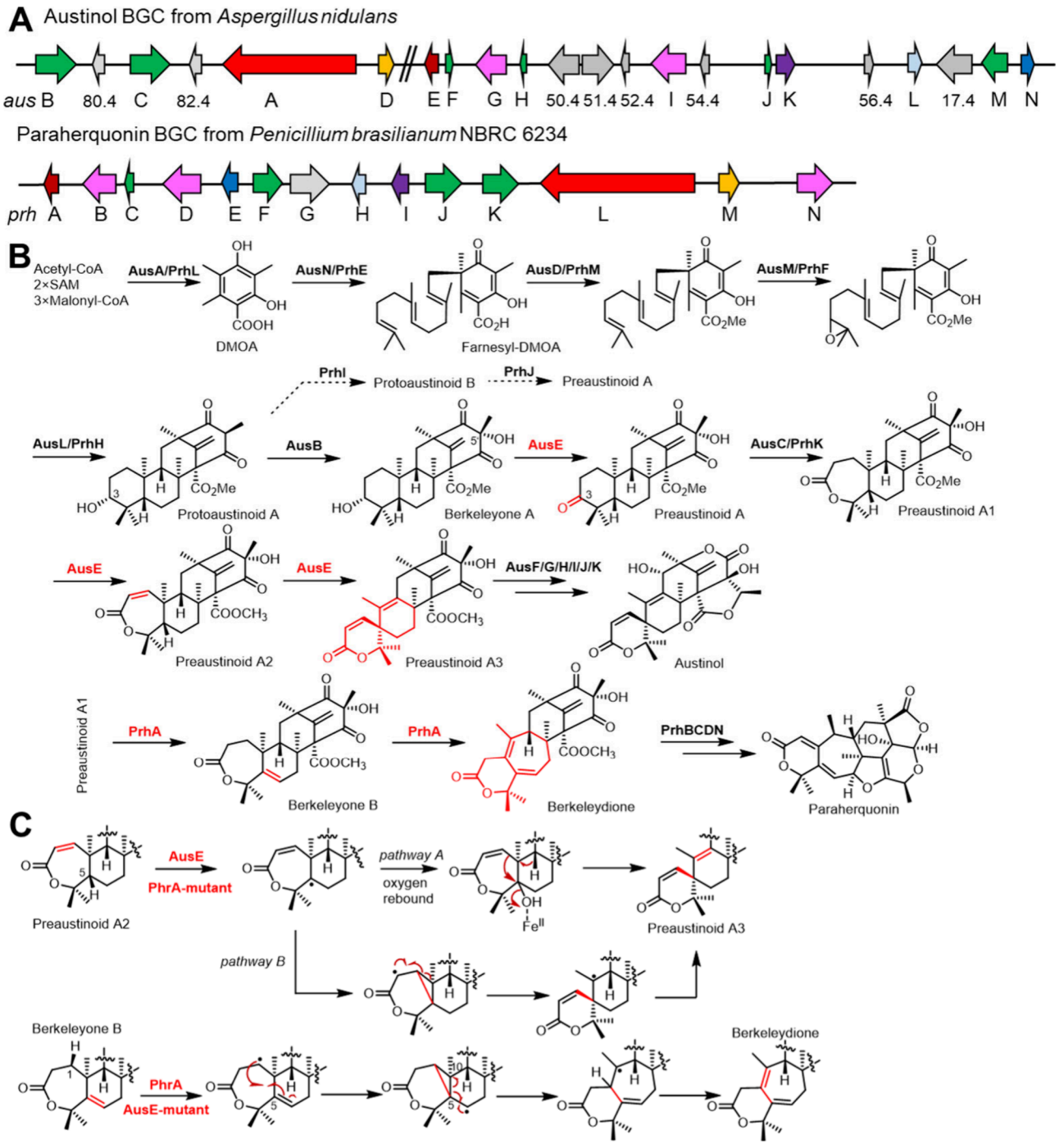

Figure 14. Biosynthesis of paraherquonin and austinol. (A) Biosynthetic gene clusters and (B) proposed biosynthetic pathway of paraherquonin and austinol. (C) The proposed mechanisms of AusE and PhrA catalyzed reactions.

5.3. PrhA and AusE in Paraherquonin and Austinol Biosynthesis

Austinol and paraherquonin also belong to a class of DOMA-derived fungal meroterpenoids (Figure 14B). Austinol can be isolated from *Aspergillus ustus* and *A. nidulans* and contains a unique spiro-lactone ring system.[146,147] Paraherquonin identified from *Penicillium paraherquei* IFO 6234 in 1982 possesses a unique cyclic molecular architecture.[148]

The austinol biosynthetic gene cluster (*aus* BGC) (Figure 14A) has been identified in *A. nidulans* and consists of two parts located in two separate regions of the chromosome.[149,150] The functions of 14 genes in the *aus* BGC have been proposed by targeted gene knockout experiments. Based on the compounds isolated from the knockout mutants combined with heterologous reconstitution in a nonproducing strain, a complete biosynthetic pathway for austinol has been proposed.[41,150,151]

The biosynthetic pathway begins with construction of the intermediate protoaustinoid A following a similar route as observed in the cases of other DMOA-derived meroterpenoids (Figure 14B).[152] Heterologous reconstruction of methyltransferase-encoding gene *aus*D in *A. oryzae* NSAR1, however, has shown that methylation of the carboxyl group of DMOA is essential prior to cyclization catalyzed by AusL.[151] Proto-

https://doi.org/10.1021/acsbiomedchemau.5c00001
ACS Bio Med Chem Au 2025, 5, 238−261

austinoid A is oxidized to berkeleyone A by another flavin-dependent monooxogenase (AusB, FMO) before dehydrogenation catalyzed by the Fe/2OG enzyme AusE generates preaustinoid A. The third FMO enzyme AusC functions as a Baeyer−Villiger monooxygenase to yield preaustinoid A1, which undergoes AsuE catalyzed desaturation and rearrangement to produce the spiro-lactone skeleton of preaustinoid A3. Finally, formation of austinol involves multiple reactions including isomerization, ketoreduction, lactonization, oxidation, and hydroxylation catalyzed by AusF/G/H/I/J/K, respectively.

The early steps of paraherquonin biosynthesis are the same as those of austinol, according to bioinformatic analysis. Furthermore, PrhI is homologous to C3 alcohol dehydrogenases in the biosynthesis of other meroterpenoids, and PrhJ and PrhK are highly similar to AusB and AusC; therefore, they have been proposed to catalyze similar oxygenations of protoaustinoid A to yield preaustinoid A1 (Figure 14B). This hypothesis has been supported by gene reconstruction in chassis *Aspergillus oryzae*.[42] The Fe/2OG enzyme PrhA may then catalyze construction of the cycloheptadiene moiety of berkeleydione from berkeleyone B. Conversion of berkeleydione to paraherquonin is proposed to be directed by three P450s (PrhB, D, and N) and one isomerase (PrhC).[42]

Possible reaction mechanisms for the various Fe/2OG enzyme catalyzed reactions in these pathways have been studied using protein structure determination and mutagenesis (Figure 14C).[153] AusE and PrhA share 72% sequence identity, and their structures are highly similar (main chain RMSD of 0.6 Å). Notably, only three residues are found to be different between the active sites of PrhA and AusE, where a double mutant V150L/A232S of PhrA switches its activity to AusE.[153] AusE catalysis has been proposed to begin with H atom abstraction from C5 which may then undergo oxygen rebound to form a hydroxylated intermediate that rearranges to preaustinoid A3 (pathway A) versus a radical mediated rearrangement (pathway B). Crystal structures of PrhA-V150L/A232S in complex with substrates including berkeleyone B, preaustinoid A1, preaustinoid A2, and preaustinoid A3 reveal that pathway B is plausible for spiro-lactone skeleton formation because of the lack of potential catalytic base near H-9 for pathway A.

A similar reaction pathway has been proposed for PhrA.[42] Due to the different A/B ring conformations, however, radical initiation begins at C1. The reaction propagates via radical addition of C1 at C5 to generate a cyclopropylcarbinyl radical species which undergoes ring opening via homolysis of the C5−C10 bond and double bond formation to yield the cycloheptadiene moiety of berkeleydione (Figure 14C).

5.4. TropC in Stipitatic Acid Biosynthesis

Tropolones represent a class of compounds with a seven-membered cyclohepta-2,4,6-trienone aromatic ring moiety.[154] Stipitatic acid is one such example of a tropolone that is isolated from *Penicillium stipitatum* in 1942[155] and structurally characterized in 1945.[156]

The biosynthetic origin of stipitatic acid is investigated through feeding experiments using isotopically labeled compounds,[157,158] and only one oxygen from O_2 is incorporated into the tropolone skeleton during the ring expansion.[159] About a decade ago, the Cox group described the biosynthesis of fungal tropolones including stipitatic acid (Figure 15A and B).[40,160,161] The stipitatic acid biosynthetic

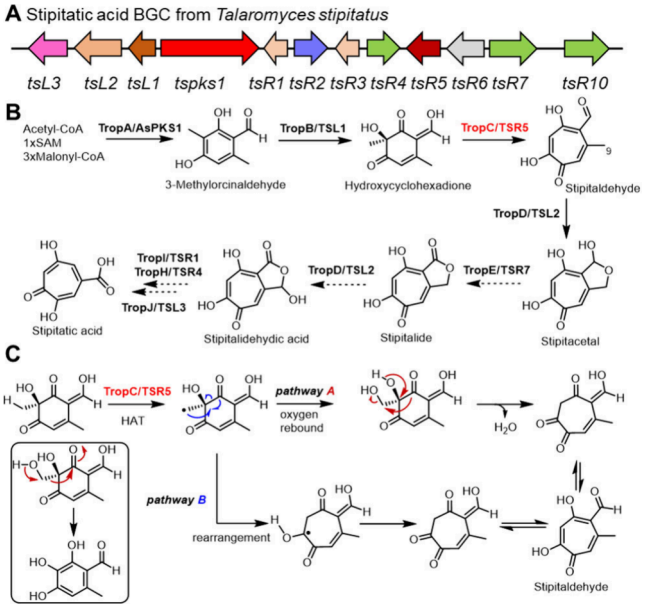

Figure 15. (A) Biosynthetic gene cluster and (B) proposed biosynthetic pathway of stipitatic acid. (C) The proposed mechanisms of the TropC catalyzed reaction. Formation of the shunt product trihydroxybenzaldehyde is shown in the box.

gene cluster from *Talaromyces stipitatus* encodes three key enzymes for the formation of the seven-membered cyclohepta-2,4,6-trienone aromatic ring. A nonreducing polyketide synthase TropA directs formation of methylorcinaldehyde,[162] which is followed by an FAD-dependent monooxygenase TropB to form a dearomatized hydroxycyclohexadione. The Fe/2OG enzyme TropC then catalyzes oxidative ring expansion to furnish the tropolone scaffold. After that, P450 monooxygenase TropD hydroxylates stipitaldehyde at C9 before nonenzymatic cyclization yields the hemiacetal stipitacetal. The following steps that convert stipitacetal into stipitatic acid remain to be established; however, a one-pot reaction with stipitalidehydic acid, NAD-dependent dehydrogenase TropH, hydrolase TropI, and decarboxylase TropJ successfully produces stipitatic acid implicating their direct involvement in stipitatic acid biosynthesis.[161]

The ring expansion catalyzed by TropC is initially proposed to proceed via Lewis' acid/base chemistry (pathway A) following Fe/2OG catalyzed hydroxylation (Figure 15C). This hypothesis is consistent with the observed shunt product trihydroxybenzaldehyde.[40] However, the Narayan group proposed an alternative mechanism where the substrate radical propagates via radical-mediated ring expansion (pathway B), which is consistent with protein structure and computational studies.[163] In addition, several residues of TropC that are critical for controlling reaction pathways between hydroxylation and ring expansion are identified through ancestral sequence reconstruction-guided strategy analysis.[164]

5.5. MtMOS in the Biosynthesis of Medicaol

Strigolactones represent a class of phytohormones produced by the roots of some plants, e.g., tomato and rice.[165] Strigolactones can be divided into canonical and noncanonical subtypes, according to their chemical structures. The structure of a canonical strigolactone is characterized by a tricyclic lactone (the ABC rings) linked to a butenolide D ring via an enol-ether bridge. These compounds can be further divided

https://doi.org/10.1021/acsbiomedchemau.5c00001
ACS Bio Med Chem Au 2025, 5, 238−261

into the strigol-type and orobanchol-type based on the stereochemistry at the BC ring junction.[165] Medicaol, an orobanchol-type strigolactone, is identified in the root exudates of *Medicago truncatula* (barrel medic). It features a special seven-membered cycloheptadiene A ring (Figure 16A).[166]

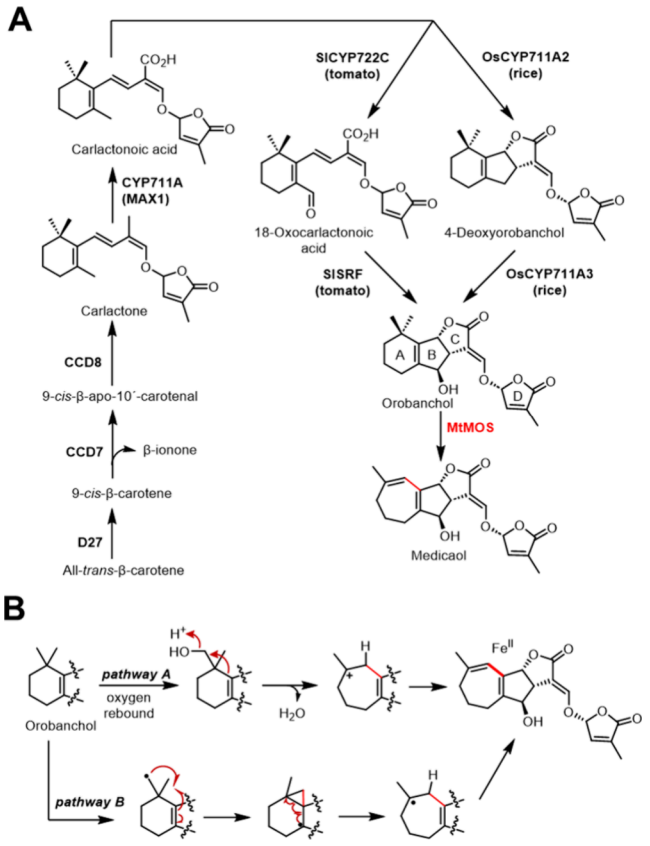

Figure 16. Biosynthesis of medicaol. (A) Proposed biosynthetic pathway of medicaol and (B) proposed reaction mechanisms of the Fe/2OG enzyme MtMOS catalyzed reaction.

The final step of medicaol biosynthesis is recently shown to be catalyzed by the Fe/2OG enzyme MtMOS with the substrate orobanchol (Figure 16A).[58] Orobanchol is generated from carlactone, which is in turn produced via D27 catalyzed isomerization from all-*trans*-*β*-carotene to 9-*cis*-*β*-carotene. This is followed by CCD7 catalyzed formation of 9-*cis*-*β*-apo-10′-carotenal, which is then converted to carlactone in the presence of CCD8.[167] Carlactone is further converted into carlactonoic acid in a reaction catalyzed by the P450 enzyme CYP711A.[168−170]

The conversion of carlactonoic acid to orobanchol was shown to proceed through two different pathways. In rice, the P450 enzyme OsCYP711A2 catalyzes stereoselective BC-ring closure to form 4-deoxyorobanchol, which is subsequently hydroxylated by OsCYP711A3.[169] In tomato, the P450 enzyme SlCYP722C catalyzes oxidation of carlactonoic acid to 18-oxocarlactonoic acid before stereoselective BC-ring formation, which is catalyzed by SlSFR, a dirigent domain-containing enzyme.[171]

Two pathways for ring expansion catalyzed by the Fe/2OG enzyme MtMOS have been proposed (Figure 16B).[58] In pathway A, the reaction starts with hydroxylation. Elimination of the hydroxyl group is proposed to trigger ring expansion through a Wagner−Meerwein rearrangement. In pathway B, ring expansion proceeds via a radical mediated pathway, where a cyclopropyl radical intermediate is produced to result in rearrangement. At the present, no detailed mechanistic studies of MtMOS catalysis have been reported.

6. C−N BOND FORMATION

6.1. TqaL Catalyzed Aziridination

Until 2024, the only Fe/2OG enzyme known to catalyze aziridination was TqaL in the biosynthetic pathway of the fungal tremorgenic mycotoxin tryptoquialanine from *Penicillium aethiopicum*.[172] Recently, several TqaL homologues together with the haloalkanoic acid dehalogenase-type hydrolase TqaF and NovR/CloR-like nonheme iron oxygenase TqaM were reported to mediate the biosynthesis of the nonproteinogenic amino acid 2-aminoisobutyric acid (AIB).[52,173,174] AIB is a building block found in many fungal natural products including atrovirdin B from *Hypocrea atroviridis*.[175] Its biosynthesis begins with an aziridination reaction catalyzed by TqaL. The reaction is followed by ring opening and subsequent oxidative decarboxylation enabled by TqaF and TqaM to form AIB (Figure 17A).

Abe's group first solved the *apo*-form crystal structure of a truncated $TqaL_{Nc}^{72-382}$ variant.[52] Biochemical assays reveal that $TqaL_{Nc}$ can use L-Val, L-Ile, and L-*allo*-Ile as substrates to produce aziridine and hydroxylated products (Figure 17A). Moreover, when (2*S*,3*S*)-4,4,4-$^2H_3$-Val is supplied as the substrate, an approximately 1:1 ratio of 2*S*,3*S*- and 2*S*,3*R*-aziridines is produced, which suggests that the C2−C3 bond undergoes rapid rotation to result in both retention and inversion of chirality at the C3.[173]

Initial mechanistic proposals to explain the aziridination reaction involve transfer of the H atom from the *β*-carbon to the Fe^{IV}=O complex (Figure 17B). Subsequent electron transfer from the radical to the Fe^{III}−OH species generates a C3 carbocation that undergoes intramolecular cyclization. An alternative mechanism, however, involves oxygen rebound to yield a *β*-hydroxylated species such that subsequent C−N bond formation takes place via an intramolecular 3-*exo*-*tet* nucleophilic substitution. Recently, the Guo and Chang groups provided experimental evidence in favor of a cationic intermediate by observing a primary deuterium KIE on the Fe^{IV}=O decay when the reaction is run with the C3-deuterated substrate isotopologue and monitored by stopped-flow absorption spectroscopy and freeze quench Mössbauer spectroscopy.[174] Moreover, distinct O origin from ^{18}O-water or O_2 at hydroxylated products that have opposite stereochemistry at the hydroxylation site supports quench of a carbocation (pathway A). Recently, the Wang group put forward a different mechanism (pathway C) based on computational studies involving conformational change of the Fe^{IV}=O complex and *N*-coordination of the substrate that would lead to a selective C−N coupling reaction.[176]

6.2. GAME33 and GAME34 in Steroidal Glycoalkaloid Biosynthesis

Steroidal glycoalkaloids (SGAs) are secondary metabolites isolated from *Solanaceous* crops such as tomato, potato, etc.[177−179] The structure of SGAs includes two components, the *N*-containing steroid aglycone unit and an oligosaccharide attached to the C-3 hydroxy group of the former moiety. The *α*-solanine and *α*-chaconine are representative SGAs that comprise ∼90% cultivated potato SGAs.[180,181] Additionally, habrochaitoside A is discovered from ripening fruit of *S.*

https://doi.org/10.1021/acsbiomedchemau.5c00001
ACS Bio Med Chem Au 2025, 5, 238−261

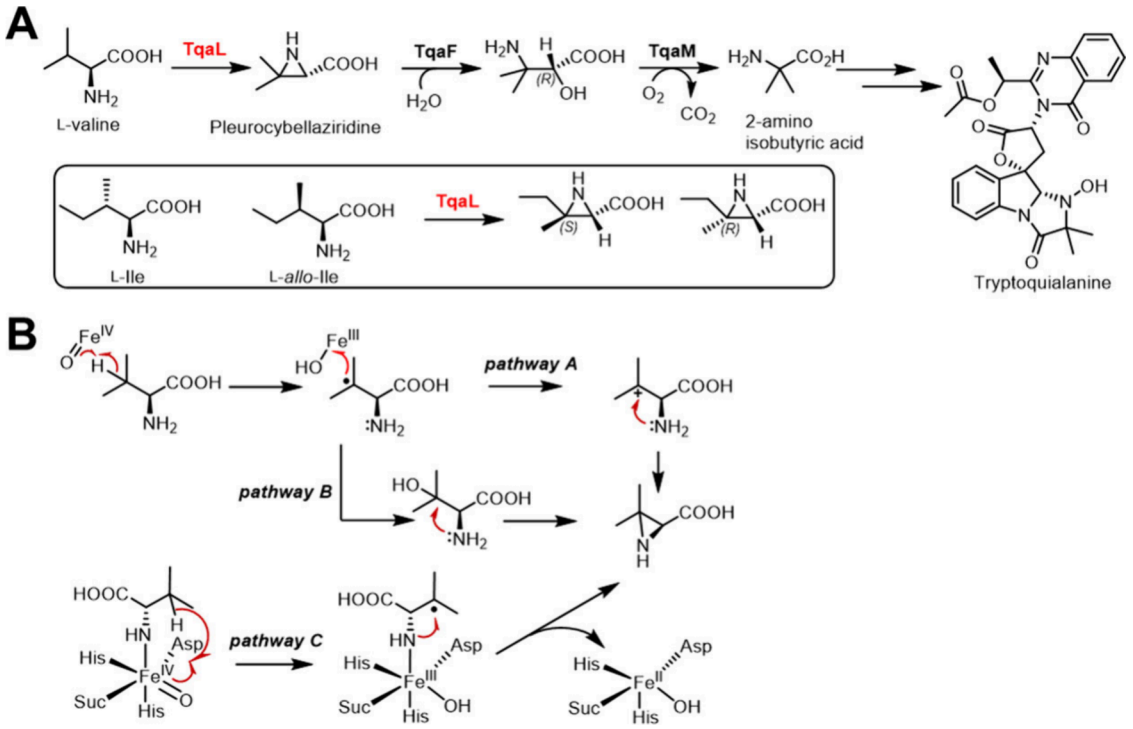

Figure 17. (A) An aziridine intermediate occurs in the proposed biosynthetic pathway of 2-aminoisobutyric acid and is formed from L-valine in an oxidation reaction catalyzed by TqaL, which can also accept other branched-chain amino acids as substrates. (B) Possible reaction mechanism of Fe/2OG enzyme TqaL.

habrochaites (a wild tomato species) and contains a unique seven-membered *N*-heterocycle (Figure 18A).[182]

Biosynthesis of SGAs begins with sequential hydroxylation of cholesterol by two P450 enzymes, GAME7 and GAME8, and one Fe/2OG enzyme GAME11 (Figure 18A).[183] Oxidization at C22 followed by E-ring closure is catalyzed by a P450 enzyme, GAME6. The resulting product is then oxidized at C26 by another P450 enzyme, GAME4. An aminotransferase, GAME12, converts the aldehyde into spirosolane-type skeleton dehydrotomatidine, where a *N*-heterocycle is formed. As a biosynthetic branch point, a 3β-hydroxysteroid dehydrogenase/$\Delta^{5,4}$ isomerase GAME25 in tomato transforms dehydrotomatidine into tomatid-4-en-3-one, which is reduced to tomatidine by the unidentified reductases.[184] This reduction generally does not occur in the potato. Finally, several uridine diphosphate-dependent glycosyltransferases catalyze glycosylation to yield α-tomatine in tomato[183] and α-solamarine and β-solamarine in potato.[185−187]

Recently, Mizutani et al. reveal that a Fe/2OG enzyme DPS-*st* from *Solanum tuberosum* directs the E- and F-ring formation of α-solamarine and β-solamarine.[188] The $^{18}O_2$-labeling experiments indicate that the oxygen at C16 does not originate from molecular oxygen. A possible reaction mechanism is proposed (Figure 18B). DPS-*st* first catalyzes C16-hydroxylation and followed by imine formation and C−O bond cleavage, resulting in 16-oxo species. A nucleophilic attack from imine to the carbonyl group forms an imine-oxy zwitterion. Additionally, Aharoni et al. report a similar reaction catalyzed by Fe/2OG enzyme GAME33 from wild tomato *S. habrochaites*. GAME33 recognizes α-tomatine and generates prashantoside A.[189] Besides, an Fe/2OG enzyme GAME34 that directs the ring-expansion of α-tomatine to form habrochaitoside A is identified where two possible pathways are considered (Figure 18C). Pathway A involves hydroxylation at C20, which serves as a leaving group during the rearrangement to yield final product. Another route includes a carbocation as key intermediate to trigger rearrangement.

7. CONCLUSION AND PERSPECTIVE

Detailed mechanistic studies have established the general importance of the Fe^{IV}=O intermediate for C−H bond activation in the catalytic cycle of Fe/2OG enzymes. However, recent studies on hydroxylation,[190] chlorination,[15,35,36,191,192] and epoxidation[21] have revealed an intricate balance between the oxygen rebound and the nonrebound pathways in defining the reaction outcomes. The Fe^{IV}=O-substrate disposition defined by the (C)H···O−Fe angle and H···O distance creates two C−H activation channels. A more obtuse (C)H···O−Fe angle (closer to linear) enables a σ-channel CH activation (the σ-pathway), while a more acute (C)H···O−Fe angle (closer to 90°) allows a π-channel C-H activation (the π-pathway). The σ-pathway appears to lead to more efficient C−H activation and may result in a closer distance between the resulting carbon radical and OH moiety of the Fe^{III}−OH species, thereby facilitating subsequent rebound to afford hydroxylation. On the other hand, the π-pathway provides a less efficient C−H activation pathway characterized by a more long-lived Fe^{IV}=O intermediate. Together with the hydrogen bonding networks provided by the secondary coordination sphere, the resulting substrate radical and Fe^{III}−OH are impaired for oxygen rebound. The π-pathway may thus bias the catalytic cycle toward nonhydroxylation outcomes including chlorination, epoxidation, and other reactions, e.g., C−C and C−N bond formations. However, factors including Fe^{IV}=O and Fe^{III}−OH orientation (offline vs online), substrate and the resulting radical position, an involvement of an assistant group on the substrate, and coordination of secondary sphere residues may also influence the reaction outcomes. Further

https://doi.org/10.1021/acsbiomedchemau.5c00001
ACS Bio Med Chem Au 2025, 5, 238−261

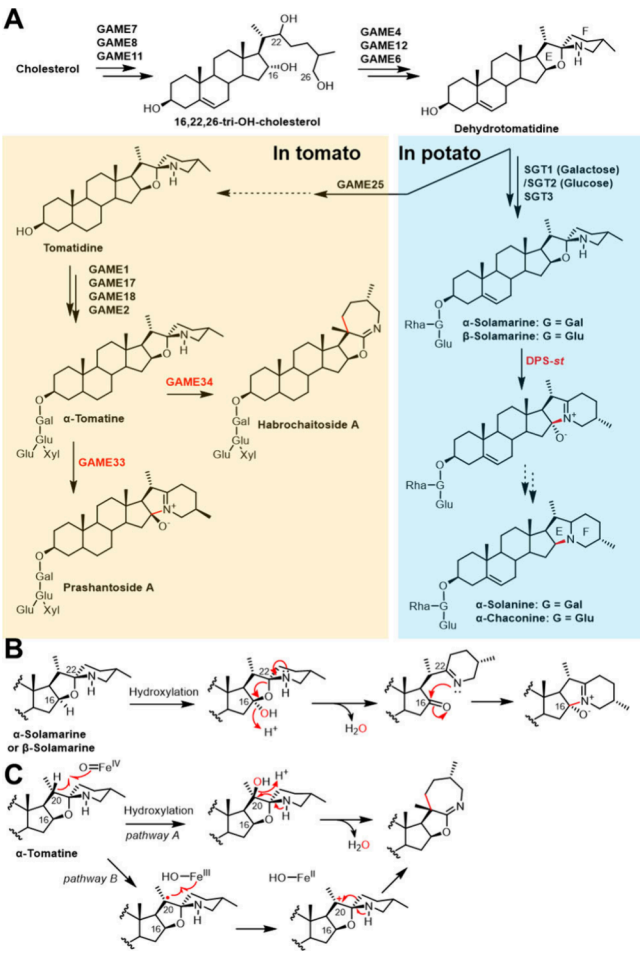

Figure 18. Biosynthesis of steroidal glycoalkaloid. (A) Proposed biosynthetic pathway of prashantoside A and habrochaitoside A in tomato and α- and β-solamarine in potato. (B–C) Possible reaction mechanisms of the Fe/2OG enzymes DPS-*st* (B) and GAME34 (C) catalyzed reactions.

exploration of these mechanistic hypotheses and their generality will help to shed light on the C–C and C–N bond forming reactions discussed in this Review, thereby providing a foundation for protein design and engineering.

In the past decade, several newly discovered Fe/2OG enzymes have been found to catalyze C–C and C–N bond forming reactions that result in strained cyclopropane and aziridine rings in addition to complex oxidative rearrangements. These reactions contribute to the late-stage modification of natural products by introducing additional structural complexity and diversity necessary for their biological properties. With further development and exploration of the biosynthetic chemistry of these enzymes and bioactive molecules, it is reasonable to predict that new Fe/2OG enzymes catalyzing unique and unexpected transformations in diverse biosynthetic pathways will continue to be discovered. Driven by investigations of the enzyme mechanisms, these studies are expected to serve as a treasure trove for the development of sustainable biocatalysts to enable useful transformations.

AUTHOR INFORMATION

Corresponding Authors

Yisong Guo – *Department of Chemistry, The Carnegie Mellon University, Pittsburgh, Pennsylvania 15213, United States;* orcid.org/0000-0002-4132-3565; Email: ysguo@andrew.cmu.edu

Wei-chen Chang – *Department of Chemistry, North Carolina State University, Raleigh, North Carolina 27695, United States;* orcid.org/0000-0002-2341-9846; Email: wchang6@ncsu.edu

Authors

Yaoyao Shen – *Department of Chemistry, North Carolina State University, Raleigh, North Carolina 27695, United States;* orcid.org/0000-0002-1785-9001

Anyi Sun – *School of Life Science and Biotechnology, Shanghai Jiao Tong University, Shanghai 200240, China*

Complete contact information is available at: https://pubs.acs.org/10.1021/acsbiomedchemau.5c00001

Notes

The authors declare no competing financial interest.

ACKNOWLEDGMENTS

The authors would like to thank Mark W. Ruszczycky for his assistance in proofreading the manuscript. This work was supported by the National Institutes of Health (NIH) GM127588 (W.-c.C. and Y.G.) and the Lord Scholar and Goodnight Early Career Innovator (W.-c.C.)

REFERENCES

(1) Yamaguchi, J.; Yamaguchi, A. D.; Itami, K. C–H bond functionalization: emerging synthetic tools for natural products and pharmaceuticals. *Angew. Chem., Int. Ed.* **2012**, *51* (36), 8960–9009.

(2) Dong, J.; Fernandez-Fueyo, E.; Hollmann, F.; Paul, C. E.; Pesic, M.; Schmidt, S.; Wang, Y.; Younes, S.; Zhang, W. Biocatalytic Oxidation Reactions: A Chemist's Perspective. *Angew. Chem., Int. Ed.* **2018**, *57* (30), 9238–9261.

(3) Li, F.; Zhang, X.; Renata, H. Enzymatic C-H functionalizations for natural product synthesis. *Curr. Opin. Chem. Biol.* **2019**, *49*, 25–32.

(4) Rose, N. R.; McDonough, M. A.; King, O. N.; Kawamura, A.; Schofield, C. J. Inhibition of 2-oxoglutarate dependent oxygenases. *Chem. Soc. Rev.* **2011**, *40* (8), 4364–4397.

(5) Martinez, S.; Hausinger, R. P. Catalytic Mechanisms of Fe(II)- and 2-Oxoglutarate-dependent Oxygenases. *J. Biol. Chem.* **2015**, *290* (34), 20702–20711.

(6) Hausinger, R. P. Biochemical Diversity of 2-Oxoglutarate-Dependent Oxygenases. In *2-Oxoglutarate-Dependent Oxygenases*; Hausinger, R. P., Schofield, C. J., Eds.; Royal Society of Chemistry: 2015; pp 1–58.

(7) Herr, C. Q.; Hausinger, R. P. Amazing Diversity in Biochemical Roles of Fe(II)/2-Oxoglutarate Oxygenases. *Trends Biochem. Sci.* **2018**, *43* (7), 517–532.

(8) Price, J. C.; Barr, E. W.; Glass, T. E.; Krebs, C.; Bollinger, J. M. Evidence for hydrogen abstraction from C1 of taurine by the high-spin Fe (IV) intermediate detected during oxygen activation by taurine: α-ketoglutarate dioxygenase (TauD). *J. Am. Chem. Soc.* **2003**, *125* (43), 13008–13009.

(9) Price, J. C.; Barr, E. W.; Tirupati, B.; Bollinger, J. M.; Krebs, C. The first direct characterization of a high-valent iron intermediate in the reaction of an α-ketoglutarate-dependent dioxygenase: a high-spin Fe (IV) complex in taurine/α-ketoglutarate dioxygenase (TauD) from Escherichia coli. *Biochemistry* **2003**, *42* (24), 7497–7508.

(10) Ryle, M. J.; Padmakumar, R.; Hausinger, R. P. Stopped-flow kinetic analysis of Escherichia coli taurine/alpha-ketoglutarate dioxygenase: interactions with alpha-ketoglutarate, taurine, and oxygen. *Biochemistry* **1999**, *38* (46), 15278−86.
(11) Dunham, N. P.; Chang, W.-c.; Mitchell, A. J.; Martinie, R. J.; Zhang, B.; Bergman, J. A.; Rajakovich, L. J.; Wang, B.; Silakov, A.; Krebs, C.; Boal, A. K.; Bollinger, J. M., Jr. Two Distinct Mechanisms for C−C Desaturation by Iron(II)- and 2-(Oxo)glutarate-Dependent Oxygenases: Importance of alpha-Heteroatom Assistance. *J. Am. Chem. Soc.* **2018**, *140* (23), 7116−7126.
(12) Liao, H. J.; Li, J.; Huang, J. L.; Davidson, M.; Kurnikov, I.; Lin, T. S.; Lee, J. L.; Kurnikova, M.; Guo, Y.; Chan, N. L.; Chang, W.-c. Insights into the Desaturation of Cyclopeptin and its C3 Epimer Catalyzed by a non-Heme Iron Enzyme: Structural Characterization and Mechanism Elucidation. *Angew. Chem., Int. Ed.* **2018**, *57* (7), 1831−1835.
(13) Chang, W.-c.; Guo, Y.; Wang, C.; Butch, S. E.; Rosenzweig, A. C.; Boal, A. K.; Krebs, C.; Bollinger, J. M., Jr Mechanism of the C5 stereoinversion reaction in the biosynthesis of carbapenem antibiotics. *Science* **2014**, *343* (6175), 1140−1144.
(14) Mitchell, A. J.; Zhu, Q.; Maggiolo, A. O.; Ananth, N. R.; Hillwig, M. L.; Liu, X.; Boal, A. K. Structural basis for halogenation by iron- and 2-oxo-glutarate-dependent enzyme WelO5. *Nat. Chem. Biol.* **2016**, *12* (8), 636−640.
(15) Wong, S. D.; Srnec, M.; Matthews, M. L.; Liu, L. V.; Kwak, Y.; Park, K.; Bell, C. B., 3rd; Alp, E. E.; Zhao, J.; Yoda, Y.; Kitao, S.; Seto, M.; Krebs, C.; Bollinger, J. M., Jr.; Solomon, E. I. Elucidation of the Fe(IV)═O intermediate in the catalytic cycle of the halogenase SyrB2. *Nature* **2013**, *499* (7458), 320−323.
(16) Vaillancourt, F. H.; Yin, J.; Walsh, C. T. SyrB2 in syringomycin E biosynthesis is a nonheme FeII alpha-ketoglutarate- and O2-dependent halogenase. *Proc. Natl. Acad. Sci. U.S.A.* **2005**, *102* (29), 10111−10116.
(17) Gama, S. R.; Stankovic, T.; Hupp, K.; Al Hejami, A.; McClean, M.; Evans, A.; Beauchemin, D.; Hammerschmidt, F.; Pallitsch, K.; Zechel, D. L. Biosynthesis of the Fungal Organophosphonate Fosfonochlorin Involves an Iron(II) and 2-(Oxo)glutarate Dependent Oxacyclase. *Chembiochem* **2022**, *23* (2), No. e202100352.
(18) Ishikawa, N.; Tanaka, H.; Koyama, F.; Noguchi, H.; Wang, C. C.; Hotta, K.; Watanabe, K. Non-heme dioxygenase catalyzes atypical oxidations of 6,7-bicyclic systems to form the 6,6-quinolone core of viridicatin-type fungal alkaloids. *Angew. Chem., Int. Ed.* **2014**, *53* (47), 12880−12884.
(19) Ushimaru, R.; Ruszczycky, M. W.; Chang, W.-c.; Yan, F.; Liu, Y. N.; Liu, H. W. Substrate Conformation Correlates with the Outcome of Hyoscyamine 6beta-Hydroxylase Catalyzed Oxidation Reactions. *J. Am. Chem. Soc.* **2018**, *140* (24), 7433−7436.
(20) Hashimoto, T.; Matsuda, J.; Yamada, Y. Two-step epoxidation of hyoscyamine to scopolamine is catalyzed by bifunctional hyoscyamine 6 beta-hydroxylase. *FEBS Lett.* **1993**, *329* (1−2), 35−39.
(21) Wenger, E. S.; Martinie, R. J.; Ushimaru, R.; Pollock, C. J.; Sil, D.; Li, A.; Hoang, N.; Palowitch, G. M.; Graham, B. P.; Schaperdoth, I.; Burke, E. J.; Maggiolo, A. O.; Chang, W.-c.; Allen, B. D.; Krebs, C.; Silakov, A.; Boal, A. K.; Bollinger, J. M., Jr. Optimized Substrate Positioning Enables Switches in the C-H Cleavage Site and Reaction Outcome in the Hydroxylation-Epoxidation Sequence Catalyzed by Hyoscyamine 6beta-Hydroxylase. *J. Am. Chem. Soc.* **2024**, *146* (35), 24271−24287.
(22) Steffan, N.; Grundmann, A.; Afiyatullov, S.; Ruan, H.; Li, S. M. FtmOx1, a non-heme Fe(II) and alpha-ketoglutarate-dependent dioxygenase, catalyses the endoperoxide formation of verruculogen in *Aspergillus fumigatus*. *Org. Biomol. Chem.* **2009**, *7* (19), 4082−4087.
(23) Chen, T.-Y.; Guo, Y.; Chang, W.-c. Iron and 2-Oxoglutarate-Dependent Isonitrile-Forming Enzymes. *Encyclopedia of Inorganic and Bioinorganic Chemistry* **2023**, No. eibc2838.
(24) Harris, N. C.; Sato, M.; Herman, N. A.; Twigg, F.; Cai, W.; Liu, J.; Zhu, X.; Downey, J.; Khalaf, R.; Martin, J.; Koshino, H.; Zhang, W. Biosynthesis of isonitrile lipopeptides by conserved nonribosomal peptide synthetase gene clusters in *Actinobacteria*. *Proc. Natl. Acad. Sci. U.S.A.* **2017**, *114* (27), 7025−7030.
(25) Wang, L.; Zhu, M.; Zhang, Q.; Zhang, X.; Yang, P.; Liu, Z.; Deng, Y.; Zhu, Y.; Huang, X.; Han, L.; Li, S.; He, J. Diisonitrile Natural Product SF2768 Functions As a Chalkophore That Mediates Copper Acquisition in *Streptomyces thioluteus*. *ACS Chem. Biol.* **2017**, *12* (12), 3067−3075.
(26) Chen, T.-Y.; Chen, J.; Tang, Y.; Zhou, J.; Guo, Y.; Chang, W.-c. Pathway from N-Alkylglycine to Alkylisonitrile Catalyzed by Iron(II) and 2-Oxoglutarate-Dependent Oxygenases. *Angew. Chem., Int. Ed.* **2020**, *59* (19), 7367−7371.
(27) Zhao, S.; Wu, L.; Xu, Y.; Nie, Y. Fe(II) and 2-oxoglutarate-dependent dioxygenases for natural product synthesis: molecular insights into reaction diversity. *Nat. Prod. Rep.* **2025**, *42*, 67.
(28) Hegg, E. L.; Que, L., Jr. The 2-His-1-carboxylate facial triad—an emerging structural motif in mononuclear non-heme iron (II) enzymes. *Eur. J. Biochem.* **1997**, *250* (3), 625−629.
(29) Blasiak, L. C.; Vaillancourt, F. H.; Walsh, C. T.; Drennan, C. L. Crystal structure of the non-haem iron halogenase SyrB2 in syringomycin biosynthesis. *Nature* **2006**, *440* (7082), 368−371.
(30) Pavel, E. G.; Zhou, J.; Busby, R. W.; Gunsior, M.; Townsend, C. A.; Solomon, E. I. Circular dichroism and magnetic circular dichroism spectroscopic studies of the non-heme ferrous active site in clavaminate synthase and its interaction with α-ketoglutarate cosubstrate. *J. Am. Chem. Soc.* **1998**, *120* (4), 743−753.
(31) Ho, R. Y.; Mehn, M. P.; Hegg, E. L.; Liu, A.; Ryle, M. J.; Hausinger, R. P.; Que, L. Resonance Raman studies of the iron (II)−α-keto acid chromophore in model and enzyme complexes. *J. Am. Chem. Soc.* **2001**, *123* (21), 5022−5029.
(32) Neidig, M. L.; Brown, C. D.; Light, K. M.; Fujimori, D. G.; Nolan, E. M.; Price, J. C.; Barr, E. W.; Bollinger, J. M., Jr; Krebs, C.; Walsh, C. T.; et al. CD and MCD of CytC3 and taurine dioxygenase: role of the facial triad in α-KG-dependent oxygenases. *J. Am. Chem. Soc.* **2007**, *129* (46), 14224−14231.
(33) Mitchell, A. J.; Dunham, N. P.; Martinie, R. J.; Bergman, J. A.; Pollock, C. J.; Hu, K.; Allen, B. D.; Chang, W.-c.; Silakov, A.; Bollinger, J. M., Jr.; Krebs, C.; Boal, A. K. Visualizing the Reaction Cycle in an Iron(II)- and 2-(Oxo)-glutarate-Dependent Hydroxylase. *J. Am. Chem. Soc.* **2017**, *139* (39), 13830−13836.
(34) Galonić, D. P.; Barr, E. W.; Walsh, C. T.; Bollinger, J. M., Jr; Krebs, C. Two interconverting Fe (IV) intermediates in aliphatic chlorination by the halogenase CytC3. *Nat. Chem. Biol.* **2007**, *3* (2), 113−116.
(35) Srnec, M.; Wong, S. D.; Matthews, M. L.; Krebs, C.; Bollinger, J. M., Jr; Solomon, E. I. Electronic Structure of the Ferryl Intermediate in the alpha-Ketoglutarate Dependent Non-Heme Iron Halogenase SyrB2: Contributions to H Atom Abstraction Reactivity. *J. Am. Chem. Soc.* **2016**, *138* (15), 5110−5122.
(36) Srnec, M.; Solomon, E. I. Frontier Molecular Orbital Contributions to Chlorination versus Hydroxylation Selectivity in the Non-Heme Iron Halogenase SyrB2. *J. Am. Chem. Soc.* **2017**, *139* (6), 2396−2407.
(37) Kastner, D. W.; Nandy, A.; Mehmood, R.; Kulik, H. J. Mechanistic insights into substrate positioning that distinguish non-heme Fe (II)/α-ketoglutarate-dependent halogenases and hydroxylases. *ACS Catal.* **2023**, *13* (4), 2489−2501.
(38) Pan, J.; Wenger, E. S.; Matthews, M. L.; Pollock, C. J.; Bhardwaj, M.; Kim, A. J.; Allen, B. D.; Grossman, R. B.; Krebs, C.; Bollinger, J. M. Evidence for Modulation of Oxygen Rebound Rate in Control of Outcome by Iron(II)- and 2-Oxoglutarate-Dependent Oxygenases. *J. Am. Chem. Soc.* **2019**, *141* (38), 15153−15165.
(39) Daum, M.; Schnell, H. J.; Herrmann, S.; Günther, A.; Murillo, R.; Müller, R.; Bisel, P.; Müller, M.; Bechthold, A. Functions of genes and enzymes involved in phenalinolactone biosynthesis. *ChemBioChem.* **2010**, *11* (10), 1383−1391.
(40) Davison, J.; al Fahad, A.; Cai, M.; Song, Z.; Yehia, S. Y.; Lazarus, C. M.; Bailey, A. M.; Simpson, T. J.; Cox, R. J. Genetic, molecular, and biochemical basis of fungal tropolone biosynthesis. *Proc. Natl. Acad. Sci. U.S.A.* **2012**, *109* (20), 7642−7647.

https://doi.org/10.1021/acsbiomedchemau.5c00001
ACS Bio Med Chem Au 2025, 5, 238−261

(41) Matsuda, Y.; Awakawa, T.; Wakimoto, T.; Abe, I. Spiro-ring formation is catalyzed by a multifunctional dioxygenase in austinol biosynthesis. *J. Am. Chem. Soc.* **2013**, *135* (30), 10962−10965.
(42) Matsuda, Y.; Iwabuchi, T.; Fujimoto, T.; Awakawa, T.; Nakashima, Y.; Mori, T.; Zhang, H.; Hayashi, F.; Abe, I. Discovery of Key Dioxygenases that Diverged the Paraherquonin and Acetoxydehydroaustin Pathways in Penicillium brasilianum. *J. Am. Chem. Soc.* **2016**, *138* (38), 12671−12677.
(43) Matsuda, Y.; Wakimoto, T.; Mori, T.; Awakawa, T.; Abe, I. Complete biosynthetic pathway of anditomin: nature's sophisticated synthetic route to a complex fungal meroterpenoid. *J. Am. Chem. Soc.* **2014**, *136* (43), 15326−15336.
(44) Nakashima, Y.; Mitsuhashi, T.; Matsuda, Y.; Senda, M.; Sato, H.; Yamazaki, M.; Uchiyama, M.; Senda, T.; Abe, I. Structural and Computational Bases for Dramatic Skeletal Rearrangement in Anditomin Biosynthesis. *J. Am. Chem. Soc.* **2018**, *140* (30), 9743−9750.
(45) Lau, W.; Sattely, E. S. Six enzymes from mayapple that complete the biosynthetic pathway to the etoposide aglycone. *Science* **2015**, *349* (6253), 1224−1228.
(46) Jakubczyk, D.; Caputi, L.; Hatsch, A.; Nielsen, C. A.; Diefenbacher, M.; Klein, J.; Molt, A.; Schroder, H.; Cheng, J. Z.; Naesby, M.; O'Connor, S. E. Discovery and reconstitution of the cycloclavine biosynthetic pathway–enzymatic formation of a cyclopropyl group. *Angew. Chem., Int. Ed.* **2015**, *54* (17), 5117−5121.
(47) Siitonen, V.; Selvaraj, B.; Niiranen, L.; Lindqvist, Y.; Schneider, G.; Metsa-Ketela, M. Divergent non-heme iron enzymes in the nogalamycin biosynthetic pathway. *Proc. Natl. Acad. Sci. U.S.A.* **2016**, *113* (19), 5251−5256.
(48) Chekan, J. R.; McKinnie, S. M. K.; Moore, M. L.; Poplawski, S. G.; Michael, T. P.; Moore, B. S. Scalable Biosynthesis of the Seaweed Neurochemical, Kainic Acid. *Angew. Chem., Int. Ed.* **2019**, *58* (25), 8454−8457.
(49) Brunson, J. K.; McKinnie, S. M.; Chekan, J. R.; McCrow, J. P.; Miles, Z. D.; Bertrand, E. M.; Bielinski, V. A.; Luhavaya, H.; Oborník, M.; Smith, G. J.; et al. Biosynthesis of the neurotoxin domoic acid in a bloom-forming diatom. *Science* **2018**, *361* (6409), 1356−1358.
(50) Lai, C. Y.; Lo, I. W.; Hewage, R. T.; Chen, Y. C.; Chen, C. T.; Lee, C. F.; Lin, S.; Tang, M. C.; Lin, H. C. Biosynthesis of Complex Indole Alkaloids: Elucidation of the Concise Pathway of Okaramines. *Angew. Chem., Int. Ed.* **2017**, *56* (32), 9478−9482.
(51) Parkinson, E. I.; Erb, A.; Eliot, A. C.; Ju, K. S.; Metcalf, W. W. Fosmidomycin biosynthesis diverges from related phosphonate natural products. *Nat. Chem. Biol.* **2019**, *15* (11), 1049−1056.
(52) Bunno, R.; Awakawa, T.; Mori, T.; Abe, I. Aziridine Formation by a Fe(II) /alpha-Ketoglutarate Dependent Oxygenase and 2-Aminoisobutyrate Biosynthesis in Fungi. *Angew. Chem., Int. Ed.* **2021**, *60* (29), 15827−15831.
(53) Shimo, S.; Ushimaru, R.; Engelbrecht, A.; Harada, M.; Miyamoto, K.; Kulik, A.; Uchiyama, M.; Kaysser, L.; Abe, I. Stereodivergent Nitrocyclopropane Formation during Biosynthesis of Belactosins and Hormaomycins. *J. Am. Chem. Soc.* **2021**, *143* (44), 18413−18418.
(54) Li, X.; Shimaya, R.; Dairi, T.; Chang, W.-c.; Ogasawara, Y. Identification of Cyclopropane Formation in the Biosyntheses of Hormaomycins and Belactosins: Sequential Nitration and Cyclopropanation by Metalloenzymes. *Angew. Chem., Int. Ed.* **2022**, *61* (7), No. e202113189.
(55) Yan, D.; Matsuda, Y. Biosynthetic Elucidation and Structural Revision of Brevione E: Characterization of the Key Dioxygenase for Pathway Branching from Setosusin Biosynthesis. *Angew. Chem., Int. Ed.* **2022**, *61* (48), No. e202210938.
(56) Wang, R.; Liang, J. J.; Yang, W.; Vuong, D.; Kalaitzis, J. A.; Lacey, A. E.; Lacey, E.; Piggott, A. M.; Chooi, Y. H.; Li, H. Heterologous Biosynthesis of the Sterol O-Acyltransferase Inhibitor Helvamide Unveils an alpha-Ketoglutarate-Dependent Cross-Linking Oxygenase. *Org. Lett.* **2024**, *26* (9), 1807−1812.
(57) Pham, M. T.; Yang, F. L.; Liu, I. C.; Liang, P. H.; Lin, H. C. Non-Heme Iron Enzymes Catalyze Heterobicyclic and Spirocyclic Isoquinolone Core Formation in Piperazine Alkaloid Biosynthesis. *Angew. Chem., Int. Ed.* **2024**, *63* (20), No. e202401324.
(58) Homma, M.; Uchida, K.; Wakabayashi, T.; Mizutani, M.; Takikawa, H.; Sugimoto, Y. 2-oxoglutarate-dependent dioxygenases and BAHD acyltransferases drive the structural diversification of orobanchol in Fabaceae plants. *Front. Plant Sci.* **2024**, *15*, No. 1392212.
(59) Thibodeaux, C. J.; Chang, W.-c.; Liu, H.-W. Enzymatic chemistry of cyclopropane, epoxide, and aziridine biosynthesis. *Chem. Rev.* **2012**, *112* (3), 1681−1709.
(60) Ushimaru, R. Three-membered ring formation catalyzed by α-ketoglutarate-dependent nonheme iron enzymes. *J. Nat. Med.* **2024**, *78* (1), 21−32.
(61) Omura, S.; Mamada, H.; Wang, N.-J.; Imamura, N.; Oiwa, R.; Iwai, Y.; Muto, N. A New Peptide Antibitoic Produed by Strepmyces Sp. *J. Antibiot.* **1984**, *37* (7), 700−705.
(62) Andres, N.; Wolf, H.; Zähner, H.; Rössner, E.; Zeeck, A.; König, W. A.; Sinnwell, V. Stoffwechselprodukte von Mikroorganismen. 253. Mitteilung. Hormaomycin, ein neues Peptid-lacton mit morphogener Aktivität auf Streptomyceten. *Helv. Chim. Acta* **1989**, *72* (3), 426−437.
(63) Asai, A.; Hasegawa, A.; Ochiai, K.; Yamashita, Y.; Mizukami, T. Belactosin A, a Novel Antituor Antibiotic Acting on Cyclin/CDK Mediated Cell Cycle Regulation, Produced by *Streptomyces* sp. *J. Antibiot.* **2000**, *53* (1), 81−83.
(64) Wolf, F.; Bauer, J. S.; Bendel, T. M.; Kulik, A.; Kalinowski, J.; Gross, H.; Kaysser, L. Biosynthesis of the beta-Lactone Proteasome Inhibitors Belactosin and Cystargolide. *Angew. Chem., Int. Ed.* **2017**, *56* (23), 6665−6668.
(65) Xu, G.; Torri, D.; Cuesta-Hoyos, S.; Panda, D.; Yates, L. R. L.; Zallot, R.; Bian, K.; Jia, D.; Iorgu, A. I.; Levy, C.; Shepherd, S. A.; Micklefield, J. Cryptic enzymatic assembly of peptides armed with beta-lactone warheads. *Nat. Chem. Biol.* **2024**, *20* (10), 1371−1379.
(66) Hofer, I.; Crusemann, M.; Radzom, M.; Geers, B.; Flachshaar, D.; Cai, X.; Zeeck, A.; Piel, J. Insights into the biosynthesis of hormaomycin, an exceptionally complex bacterial signaling metabolite. *Chem. Biol.* **2011**, *18* (3), 381−391.
(67) Heide, L.; Westrich, L.; Anderle, C.; Gust, B.; Kammerer, B.; Piel, J. Use of a halogenase of hormaomycin biosynthesis for formation of new clorobiocin analogues with 5-chloropyrrole moieties. *Chembiochem* **2008**, *9* (12), 1992−9.
(68) Colabroy, K. L.; Hackett, W. T.; Markham, A. J.; Rosenberg, J.; Cohen, D. E.; Jacobson, A. Biochemical characterization of L-DOPA 2, 3-dioxygenase, a single-domain type I extradiol dioxygenase from lincomycin biosynthesis. *Arch. Biochem. Biophys.* **2008**, *479* (2), 131−138.
(69) Beller, P.; Fink, P.; Wolf, F.; Mannle, D.; Helmle, I.; Kuttenlochner, W.; Unterfrauner, D.; Engelbrecht, A.; Staudt, N. D.; Kulik, A.; Groll, M.; Gross, H.; Kaysser, L. Characterization of the cystargolide biosynthetic gene cluster and functional analysis of the methyltransferase CysG. *J. Biol. Chem.* **2024**, *300* (1), No. 105507.
(70) Engelbrecht, A.; Wolf, F.; Esch, A.; Kulik, A.; Kozhushkov, S. I.; de Meijere, A.; Hughes, C. C.; Kaysser, L. Discovery of a Cryptic Nitro Intermediate in the Biosynthesis of the 3-(trans-2′-Aminocyclopropyl)alanine Moiety of Belactosin A. *Org. Lett.* **2022**, *24* (2), 736−740.
(71) Pang, L.; Niu, W.; Duan, Y.; Huo, L.; Li, A.; Wu, J.; Zhang, Y.; Bian, X.; Zhong, G. In vitro characterization of a nitro-forming oxygenase involved in 3-(trans-2′-aminocyclopropyl)alanine biosynthesis. *Eng. Mcrobiol.* **2022**, *2* (1), No. 100007.
(72) Ushimaru, R.; Cha, L.; Shimo, S.; Li, X.; Paris, J. C.; Mori, T.; Miyamoto, K.; Coffer, L.; Uchiyama, M.; Guo, Y.; Chang, W.-c.; Abe, I. Mechanistic Analysis of Stereodivergent Nitroalkane Cyclopropanation Catalyzed by Nonheme Iron Enzymes. *J. Am. Chem. Soc.* **2023**, *145* (44), 24210−24217.
(73) Jakubczyk, D.; Cheng, J. Z.; O'Connor, S. E. Biosynthesis of the ergot alkaloids. *Nat. Prod. Rep.* **2014**, *31* (10), 1328−1338.
(74) Stauffacher, D.; Niklaus, P.; Tscherter, H.; Weber, H.; Hofmann, A. Cycloclavin, ein neues alkaloid aus Ipomoea

https://doi.org/10.1021/acsbiomedchemau.5c00001
ACS Bio Med Chem Au 2025, 5, 238−261

hildebrandtii vatke—71: Mutterkornalkaloide. *Tetrahedron* **1969**, *25* (24), 5879−5887.
(75) Furuta, T.; Koike, M.; Abe, M. Isolation of Cycloclavine from the Culture Broth of *Aspergillus japonicus* SAITO. *Agric. Biol. Chem.* **1982**, *46* (7), 1921−1922.
(76) Jakubczyk, D.; Caputi, L.; Stevenson, C. E.; Lawson, D. M.; O'Connor, S. E. Structural characterization of EasH (*Aspergillus japonicus*) - an oxidase involved in cycloclavine biosynthesis. *Chem. Commun.* **2016**, *52* (99), 14306−14309.
(77) Yan, L.; Liu, Y. Insights into the Mechanism and Enantioselectivity in the Biosynthesis of Ergot Alkaloid Cycloclavine Catalyzed by Aj_EasH from *Aspergillus japonicus*. *Inorg. Chem.* **2019**, *58* (20), 13771−13781.
(78) Macias, F. A.; Varela, R. M.; Simonet, A. M.; Cutler, H. G.; Cutler, S. J.; Dugan, F. M.; Hill, R. A. Novel bioactive breviane spiroditerpenoids from *Penicillium brevicompactum* Dierckx. *J. Org. Chem.* **2000**, *65* (26), 9039−9046.
(79) Wei, X.; Matsuyama, T.; Sato, H.; Yan, D.; Chan, P. M.; Miyamoto, K.; Uchiyama, M.; Matsuda, Y. Molecular and Computational Bases for Spirofuranone Formation in Setosusin Biosynthesis. *J. Am. Chem. Soc.* **2021**, *143* (42), 17708−17715.
(80) Gebhardt, K.; Meyer, S. W.; Schinko, J.; Bringmann, G.; Zeeck, A.; Fiedler, H.-P. Phenalinolactones A−D, terpenoglycoside antibiotics from *Streptomyces* sp. Tü 6071. *J. Antibiot.* **2011**, *64* (3), 229−232.
(81) Gebhardt, K. *Dissertation*, Institute of Microbiology, University of Tübingen: Germany, 2002.
(82) Meyer, S. *Dissertation*, Institute of Organic and Biomolecular Chemistry, University of Göttingen: Germany, 2003.
(83) Dürr, C.; Schnell, H.-J.; Luzhetskyy, A.; Murillo, R.; Weber, M.; Welzel, K.; Vente, A.; Bechthold, A. Biosynthesis of the terpene phenalinolactone in *Streptomyces* sp. Tü6071: analysis of the gene cluster and generation of derivatives. *Chem. Biol.* **2006**, *13* (4), 365−377.
(84) Binz, T. M.; Wenzel, S. C.; Schnell, H. J.; Bechthold, A.; Müller, R. Heterologous expression and genetic engineering of the phenalinolactone biosynthetic gene cluster by using red/ET recombineering. *Chembiochem* **2008**, *9* (3), 447−454.
(85) Alsup, T. A.; Li, Z.; McCadden, C. A.; Jagels, A.; Łomowska-Keehner, D. P.; Marshall, E. M.; Dong, L.-B.; Loesgen, S.; Rudolf, J. D. Early-stage biosynthesis of phenalinolactone diterpenoids involves sequential prenylation, epoxidation, and cyclization. *RSC Chem. Biol.* **2024**, *5* (10), 1010−1016.
(86) Werner, P.; Voigt, M.; Keinänen, K.; Wisden, W.; Seeburg, P. H. Cloning of a putative high-affinity kainate receptor expressed predominantly in hippocampal CA3 cells. *Nature* **1991**, *351* (6329), 742−744.
(87) Trainer, V. L.; Bates, S. S.; Lundholm, N.; Thessen, A. E.; Cochlan, W. P.; Adams, N. G.; Trick, C. G. Pseudo-nitzschia physiological ecology, phylogeny, toxicity, monitoring and impacts on ecosystem health. *Harmful algae* **2012**, *14*, 271−300.
(88) Tian, Z.; Clark, B. L.; Menard, F. Kainic acid-based agonists of glutamate receptors: SAR analysis and guidelines for analog design. *ACS Chem. Neurosci.* **2019**, *10* (10), 4190−4198.
(89) Nitta, I.; Watase, H.; Tomiie, Y. Structure of kainic acid and its isomer, allokainic acid. *Nature* **1958**, *181* (4611), 761−762.
(90) Ramsey, U. P.; Douglas, D. J.; Walter, J. A.; Wright, J. L. Biosynthesis of domoic acid by the diatom Pseudo-nitzschia multiseries. *Nat. toxins* **1998**, *6* (3−4), 137−146.
(91) Savage, T. J.; Smith, G. J.; Clark, A. T.; Saucedo, P. N. Condensation of the isoprenoid and amino precursors in the biosynthesis of domoic acid. *Toxicon* **2012**, *59* (1), 25−33.
(92) Steele, T. S.; Brunson, J. K.; Maeno, Y.; Terada, R.; Allen, A. E.; Yotsu-Yamashita, M.; Chekan, J. R.; Moore, B. S. Domoic acid biosynthesis in the red alga Chondria armata suggests a complex evolutionary history for toxin production. *Proc. Natl. Acad. Sci. U.S.A.* **2022**, *119* (6), No. e2117407119.
(93) Hopiavuori, A. R.; McKinnie, S. M. K. Algal Kainoid Synthases Exhibit Substrate-Dependent Hydroxylation and Cyclization Activities. *ACS Chem. Biol.* **2023**, *18* (12), 2457−2463.
(94) Chen, T.-Y.; Xue, S.; Tsai, W.-C.; Chien, T.-C.; Guo, Y.; Chang, W.-c. Deciphering Pyrrolidine and Olefin Formation Mechanism in Kainic Acid Biosynthesis. *ACS Catal.* **2021**, *11* (1), 278−282.
(95) Borsche, W.; Niemann, J. Über Podophyllin. *Justus Liebigs Ann. Chem.* **1932**, *494* (1), 126−142.
(96) Yu, X.; Che, Z.; Xu, H. Recent Advances in the Chemistry and Biology of Podophyllotoxins. *Chemistry−A European Journal* **2017**, *23* (19), 4467−4526.
(97) Shah, Z.; Gohar, U. F.; Jamshed, I.; Mushtaq, A.; Mukhtar, H.; Zia-Ui-Haq, M.; Toma, S. I.; Manea, R.; Moga, M.; Popovici, B. Podophyllotoxin: History, Recent Advances and Future Prospects. *Biomolecules* **2021**, *11* (4), 603.
(98) Shen, S.; Tong, Y.; Luo, Y.; Huang, L.; Gao, W. Biosynthesis, total synthesis, and pharmacological activities of aryltetralin-type lignan podophyllotoxin and its derivatives. *Nat. Prod. Rep.* **2022**, *39* (9), 1856−1875.
(99) Davin, L. B.; Wang, H.-B.; Crowell, A. L.; Bedgar, D. L.; Martin, D. M.; Sarkanen, S.; Lewis, N. G. Stereoselective bimolecular phenoxy radical coupling by an auxiliary (dirigent) protein without an active center. *Science* **1997**, *275* (5298), 362−367.
(100) Chu, A.; Dinkova, A.; Davin, L. B.; Bedgar, D. L.; Lewis, N. G. Stereospecificity of (+)-pinoresinol and (+)-lariciresinol reductases from Forsythia intermedia. *J. Biol. Chem.* **1993**, *268* (36), 27026−27033.
(101) Moinuddin, S. G.; Youn, B.; Bedgar, D. L.; Costa, M. A.; Helms, G. L.; Kang, C.; Davin, L. B.; Lewis, N. G. Secoisolariciresinol dehydrogenase: mode of catalysis and stereospecificity of hydride transfer in *Podophyllum peltatum*. *Org. Biomol. Chem.* **2006**, *4* (5), 808−816.
(102) Marques, J. V.; Kim, K. W.; Lee, C.; Costa, M. A.; May, G. D.; Crow, J. A.; Davin, L. B.; Lewis, N. G. Next generation sequencing in predicting gene function in podophyllotoxin biosynthesis. *J. Biol. Chem.* **2013**, *288* (1), 466−479.
(103) Chang, W.-c.; Yang, Z. J.; Tu, Y. H.; Chien, T. C. Reaction Mechanism of a Nonheme Iron Enzyme Catalyzed Oxidative Cyclization via C-C Bond Formation. *Org. Lett.* **2019**, *21* (1), 228−232.
(104) Tang, H.; Wu, M. H.; Lin, H. Y.; Han, M. R.; Tu, Y. H.; Yang, Z. J.; Chien, T. C.; Chan, N. L.; Chang, W.-c. Mechanistic analysis of carbon-carbon bond formation by deoxypodophyllotoxin synthase. *Proc. Natl. Acad. Sci. U.S.A.* **2022**, *119* (1), No. e2113770119.
(105) Ingold, Z.; Grogan, G.; Lichman, B. R. Structure and mutation of deoxypodophyllotoxin synthase (DPS) from *Podophyllum hexandrum*. *Front. Catal.* **2023**, *3*, No. 1178345.
(106) Hardy, F. G.; Wong, H. P. H.; de Visser, S. P. Computational Study Into the Oxidative Ring-Closure Mechanism During the Biosynthesis of Deoxypodophyllotoxin. *Chemistry−A European Journal* **2024**, *30* (22), No. e202400019.
(107) Su, Y.; Lai, W. Unraveling the Mechanism of the Oxidative C-C Bond Coupling Reaction Catalyzed by Deoxypodophyllotoxin Synthase. *Inorg. Chem.* **2024**, *63* (30), 13948−13958.
(108) Hayashi, H.; Takiuchi, K.; Murao, S.; Arai, M. Structure and Insecticidal Activity of New Indole Alkaloids, Okaramines A and B, from *Penicillium simplicissimum* AK-40. *Agric. Biol. Chem.* **1989**, *53* (2), 461−469.
(109) Hayashi, H.; Fujiwara, T.; Murao, S.; Arai, M. Okaramine C, a New Insecticidal Indole Alkaloid from *Penicillium simplicissimum*. *Agric. Biol. Chem.* **1991**, *55* (12), 3143−3145.
(110) Hayashi, H.; Asabu, Y.; Murao, S.; Arai, M. New okaramine congeners, okaramines D, E, and F, from *Penicillium simplicissimum* ATCC 90288. *Biosci. Biotechnol. Biochem.* **1995**, *59* (2), 246−250.
(111) Hayashi, H.; Sakaguchi, A. Okaramine G, a New Okaramine Congener from *Penicillium simplicissimum* ATCC 90288. *Biosci. Biotechnol. Biochem.* **1998**, *62* (4), 804−806.

(112) Hayashi, H.; Furutsuka, K.; Shiono, Y. Okaramines H and I, new okaramine congeners, from *Aspergillus aculeatus*. *J. Nat. Prod.* **1999**, *62* (2), 315−317.
(113) Shiono, Y.; Akiyama, K.; Hayashi, H. New okaramine congeners, okamines J, K, L, M and related compounds, from *Penicillium simplicissimum* ATCC 90288. *Biosci. Biotechnol. Biochem.* **1999**, *63* (11), 1910−1920.
(114) Shiono, Y.; Akiyama, K.; Hayashi, H. Effect of the azetidine and azocine rings of okaramine B on insecticidal activity. *Biosci. Biotechnol. Biochem.* **2000**, *64* (7), 1519−1521.
(115) Wang, Y.; Chen, L.; Fang, W.; Zeng, Z.; Wu, Z.; Liu, F.; Liu, X.; Gong, Y.; Zhu, L.; Wang, K. Genomic and Comparative Transcriptomic Analyses Reveal Key Genes Associated with the Biosynthesis Regulation of Okaramine B in *Penicillium daleae* NBP-49626. *Int. J. Mol. Sci.* **2024**, DOI: 10.3390/ijms25041965.
(116) Bhuyan, B. Fermentation, taxonomic and biological studies of nogalamycin. *Antimicrob. Ag. Chemother.* **1965**, 836−844.
(117) Wiley, P.; MacKellar, F.; Caron, E.; Kelly, R. Isolation, characterization and degradation of nogalamycin. *Tetrahedron Lett.* **1968**, *9* (6), 663−668.
(118) Wiley, P. F.; Kelly, R. B.; Caron, E. L.; Wiley, V. H.; Johnson, J. H.; MacKellar, F. A.; Mizsak, S. A. Structure of nogalamycin. *J. Am. Chem. Soc.* **1977**, *99* (2), 542−549.
(119) Ylihonko, K.; Hakala, J.; Kunnari, T.; Mäntsälälä, P. Production of hybrid anthracycline antibiotics by heterologous expression of Streptomyces nogalater nogalamycin biosynthesis genes. *Microbiology* **1996**, *142* (8), 1965−1972.
(120) Ylihonko, K.; Tuikkanen, J.; Jussila, S.; Cong, L.; Mäntsälä, P. A gene cluster involved in nogalamycin biosynthesis from *Streptomyces nogalater*: sequence analysis and complementation of early-block mutations in the anthracycline pathway. *Mol. Gen. Genetics* **1996**, *251*, 113−120.
(121) Torkkell, S.; Ylihonko, K.; Hakala, J.; Skurnik, M.; Mäntsälä, P. Characterization of *Streptomyces nogalater* genes encoding enzymes involved in glycosylation steps in nogalamycin biosynthesis. *Mol. Genet. Genomics* **1997**, *256*, 203−209.
(122) Kantola, J.; Kunnari, T.; Hautala, A.; Hakala, J.; Ylihonko, K.; Mäntsälä, P. Elucidation of anthracyclinone biosynthesis by stepwise cloning of genes for anthracyclines from three different *Streptomyces* sp. *Microbiology* **2000**, *146* (1), 155−163.
(123) Torkkell, S.; Kunnari, T.; Palmu, K.; Hakala, J.; Mäntsälä, P.; Ylihonko, K. Identification of a cyclase gene dictating the C-9 stereochemistry of anthracyclines from *Streptomyces nogalater*. *Antimicrob. Agents Chemother.* **2000**, *44* (2), 396−399.
(124) Torkkell, S.; Kunnari, T.; Palmu, K.; Mantsala, P.; Hakala, J.; Ylihonko, K. The entire nogalamycin biosynthetic gene cluster of *Streptomyces nogalater*: characterization of a 20-kb DNA region and generation of hybrid structures. *Mol. Genet. Genomics* **2001**, *266* (2), 276−288.
(125) Metsä-Ketelä, M.; Niemi, J.; Mäntsälä, P.; Schneider, G. *Anthracycline biosynthesis: genes, enzymes and mechanisms*; Springer: 2008; pp 101−140.
(126) Hulst, M. B.; Grocholski, T.; Neefjes, J. J. C.; van Wezel, G. P.; Metsa-Ketela, M. Anthracyclines: biosynthesis, engineering and clinical applications. *Nat. Prod. Rep.* **2022**, *39* (4), 814−841.
(127) Siitonen, V.; Blauenburg, B.; Kallio, P.; Mantsala, P.; Metsa-Ketela, M. Discovery of a two-component monooxygenase SnoaW/SnoaL2 involved in nogalamycin biosynthesis. *Chem. Biol.* **2012**, *19* (5), 638−646.
(128) Nji Wandi, B.; Siitonen, V.; Palmu, K.; Metsa-Ketela, M. The Rieske Oxygenase SnoT Catalyzes 2″-Hydroxylation of l-Rhodosamine in Nogalamycin Biosynthesis. *Chembiochem* **2020**, *21* (21), 3062−3066.
(129) Nji Wandi, B.; Siitonen, V.; Dinis, P.; Vukic, V.; Salminen, T. A.; Metsa-Ketela, M. Evolution-guided engineering of non-heme iron enzymes involved in nogalamycin biosynthesis. *FEBS J.* **2020**, *287* (14), 2998−3011.
(130) Wang, R.; Piggott, A. M.; Chooi, Y. H.; Li, H. Discovery, bioactivity and biosynthesis of fungal piperazines. *Nat. Prod. Rep.* **2023**, *40* (2), 387−411.
(131) Li, H.; Lacey, A. E.; Shu, S.; Kalaitzis, J. A.; Vuong, D.; Crombie, A.; Hu, J.; Gilchrist, C. L. M.; Lacey, E.; Piggott, A. M.; Chooi, Y. H. Hancockiamides: phenylpropanoid piperazines from Aspergillus hancockii are biosynthesised by a versatile dual single-module NRPS pathway. *Org. Biomol. Chem.* **2021**, *19* (3), 587−595.
(132) Iguchi, E.; Okuhara, M.; Kohsaka, M.; Aoki, H.; Imanaka, H. Studies on new phosphonic acid antibiotics II. Taxonomic studies on producing organisms of the phosphonic acid and related compounds. *J. Antibiot.* **1980**, *33* (1), 18−23.
(133) Kuroda, Y.; Okuhara, M.; Goto, T.; Okamoto, M.; Terano, H.; Kohsaka, M.; Aoki, H.; Imanaka, H. Studies on new phosphonic acid antibiotics IV. structure determination of FR-33289, FR-31564 AND FR-32863. *J. Antibiot.* **1980**, *33* (1), 29−35.
(134) Okuhara, M.; Kuroda, Y.; Goto, T.; Okamoto, M.; Terano, H.; Kohsaka, M.; Aoki, H.; Imanaka, H. Studies on new phosphonic acid antibiotics III. isolation and characterization of FR-31564. *J. Antibiot.* **1980**, *33* (1), 24−28.
(135) Horsman, G. P.; Zechel, D. L. Phosphonate Biochemistry. *Chem. Rev.* **2017**, *117* (8), 5704−5783.
(136) Li, X.; Xue, S.; Guo, Y.; Chang, W.-v. Mechanism of Methyldehydrofosmidomycin Maturation: Use Olefination to Enable Chain Elongation. *J. Am. Chem. Soc.* **2022**, *144* (18), 8257−8266.
(137) Parkinson, E. I.; Lakkis, H. G.; Alwali, A. A.; Metcalf, M. E. M.; Modi, R.; Metcalf, W. W. An Unusual Oxidative Rearrangement Catalyzed by a Divergent Member of the 2-Oxoglutarate-Dependent Dioxygenase Superfamily during Biosynthesis of Dehydrofosmidomycin. *Angew. Chem., Int. Ed.* **2022**, *61* (30), No. e202206173.
(138) Bai, T.; Matsuda, Y.; Tao, H.; Mori, T.; Zhang, Y.; Abe, I. Structural Diversification of Andiconin-Derived Natural Products by alpha-Ketoglutarate-Dependent Dioxygenases. *Org. Lett.* **2020**, *22* (11), 4311−4315.
(139) Simpson, T. J.; Walkinshaw, M. D. Anditomin, a new C 25 metabolite from Aspergillus variecolor. *Chem. Commun.* **1981**, No. 17, 914−915.
(140) Simpson, T. J. Biosynthesis of highly modified meroterpenoids in *Aspergillus variecolor*. Incorporation of 13C-labelled acetates and methionine into anditomin and andilesin C. *Tetrahedron Lett.* **1981**, *22* (38), 3785−3788.
(141) Mclntyre, C. R.; Scott, F. E.; Simpson, T. J.; Trimble, L. A.; Vederas, J. C. Biosynthesis of the meroterpenoid metabolite, andilesin A, by Aspergillus variecolor: origins of the oxygen atoms. *Chem. Commun.* **1986**, No. 7, 501−503.
(142) Simpson, T. J.; Ahmed, S. A.; McIntyre, C. R.; Scott, F. E.; Sadler, I. H. Biosynthesis of polyketide-terpenoid (meroterpenoid) metabolites andibenin B and andilesin A in *Aspergillus variecolor*. *Tetrahedron* **1997**, *53* (11), 4013−4034.
(143) Li, Q.; Chen, C.; Cheng, L.; Wei, M.; Dai, C.; He, Y.; Gong, J.; Zhu, R.; Li, X. N.; Liu, J.; Wang, J.; Zhu, H.; Zhang, Y. Emeridones A-F, a Series of 3,5-Demethylorsellinic Acid-Based Meroterpenoids with Rearranged Skeletons from an Endophytic Fungus *Emericella* sp. TJ29. *J. Org. Chem.* **2019**, *84* (3), 1534−1541.
(144) He, Y.; Hu, Z.; Li, Q.; Huang, J.; Li, X. N.; Zhu, H.; Liu, J.; Wang, J.; Xue, Y.; Zhang, Y. Bioassay-Guided Isolation of Antibacterial Metabolites from *Emericella* sp. TJ29. *J. Nat. Prod.* **2017**, *80* (9), 2399−2405.
(145) Tao, H.; Mori, T.; Chen, H.; Lyu, S.; Nonoyama, A.; Lee, S.; Abe, I. Molecular insights into the unusually promiscuous and catalytically versatile Fe(II)/alpha-ketoglutarate-dependent oxygenase SptF. *Nat. Commun.* **2022**, *13* (1), 95.
(146) Simpson, T. J.; Stenzel, D. J.; Bartlett, A. J.; O'Brien, E.; Holker, J. S. Studies on fungal metabolites. Part 3. 13 C Nmr spectral and structural studies on austin and new related meroterpenoids from *Aspergillus ustus*, *Aspergillus variecolor*, and *Penicillium diversum*. *J. Chem. Soc., Perkin Trans.* **1982**, *1*, 2687−2692.
(147) Szewczyk, E.; Chiang, Y.-M.; Oakley, C. E.; Davidson, A. D.; Wang, C. C.; Oakley, B. R. Identification and characterization of the

asperthecin gene cluster of *Aspergillus nidulans*. *Appl. Environ. Microbiol.* **2008**, *74* (24), 7607−7612.
(148) Okuyama, E.; Yamazaki, M.; Kobayashi, K.; Sakurai, T. Paraherquonin, a new meroterpenoid from *Penicillium paraherquei*. *Tetrahedron Lett.* **1983**, *24* (30), 3113−3114.
(149) Nielsen, M. L.; Nielsen, J. B.; Rank, C.; Klejnstrup, M. L.; Holm, D. K.; Brogaard, K. H.; Hansen, B. G.; Frisvad, J. C.; Larsen, T. O.; Mortensen, U. H. A genome-wide polyketide synthase deletion library uncovers novel genetic links to polyketides and meroterpenoids in *Aspergillus nidulans*. *FEMS Microbiol Lett.* **2011**, *321* (2), 157−166.
(150) Lo, H. C.; Entwistle, R.; Guo, C. J.; Ahuja, M.; Szewczyk, E.; Hung, J. H.; Chiang, Y. M.; Oakley, B. R.; Wang, C. C. Two separate gene clusters encode the biosynthetic pathway for the meroterpenoids austinol and dehydroaustinol in *Aspergillus nidulans*. *J. Am. Chem. Soc.* **2012**, *134* (10), 4709−4720.
(151) Matsuda, Y.; Awakawa, T.; Itoh, T.; Wakimoto, T.; Kushiro, T.; Fujii, I.; Ebizuka, Y.; Abe, I. Terretonin biosynthesis requires methylation as essential step for cyclization. *Chembiochem* **2012**, *13* (12), 1738−1741.
(152) Matsuda, Y.; Abe, I. Biosynthesis of fungal meroterpenoids. *Nat. Prod. Rep.* **2016**, *33* (1), 26−53.
(153) Nakashima, Y.; Mori, T.; Nakamura, H.; Awakawa, T.; Hoshino, S.; Senda, M.; Senda, T.; Abe, I. Structure function and engineering of multifunctional non-heme iron dependent oxygenases in fungal meroterpenoid biosynthesis. *Nat. Commun.* **2018**, *9* (1), 104.
(154) Guo, H.; Roman, D.; Beemelmanns, C. Tropolone natural products. *Nat. Prod. Rep.* **2019**, *36* (8), 1137−1155.
(155) Birkinshaw, J. H.; Chambers, A. R.; Raistrick, H. Studies in the biochemistry of micro-organisms: Stipitatic acid, C8H6O5, a metabolic product of *Penicillium stipitatum* Thom. *Biochem. J.* **1942**, *36* (1−2), 242−251.
(156) Dewar, M. J. Structure of stipitatic acid. *Nature* **1945**, *155* (3924), 50−51.
(157) Bentley, R. Biosynthesis of Tropolones in Penicillium stipitatum: III. Tracer studies on the formation on stipitatonic and stipitatic acids. *J. Biol. Chem.* **1963**, *238* (5), 1895−1902.
(158) Bryant, R. W., Jr; Light, R. Stipitatonic acid biosynthesis. Incorporation of [formyl-14C]-3-methylorcylaldehyde and carbon-14-labeled stipitaldehydic acid, a new tropolone metabolite. *Biochemistry* **1974**, *13* (7), 1516−1522.
(159) Osullivan, M. C.; Schwab, J. M. Verification of the mechanism of oxidative ring expansion in the biosynthesis of stipitatic acid by *Talaromyces stipitatus*. *Bioorg. Chem.* **1995**, *23* (2), 131−143.
(160) Cox, R. J.; Al-Fahad, A. Chemical mechanisms involved during the biosynthesis of tropolones. *Curr. Opin. Chem. Biol.* **2013**, *17* (4), 532−536.
(161) al Fahad, A.; Abood, A.; Simpson, T. J.; Cox, R. J. The biosynthesis and catabolism of the maleic anhydride moiety of stipitatonic acid. *Angew. Chem., Int. Ed.* **2014**, *53* (29), 7519−7523.
(162) Bailey, A. M.; Cox, R. J.; Harley, K.; Lazarus, C. M.; Simpson, T. J.; Skellam, E. Characterisation of 3-methylorcinaldehyde synthase (MOS) in *Acremonium strictum*: first observation of a reductive release mechanism during polyketide biosynthesis. *Chem. Commun.* **2007**, No. 39, 4053−4055.
(163) Doyon, T. J.; Skinner, K.; Yang, D.; Mallik, L.; Wymore, T.; Koutmos, M.; Zimmerman, P. M.; Narayan, A. Radical tropolone biosynthesis. *ChemRxiv* **2020**, DOI: 10.26434/chemrxiv.12780044.v1.
(164) Yang, D.; Chiang, C. H.; Wititsuwannakul, T.; Brooks, C. L.; Zimmerman, P. M.; Narayan, A. R. H. Engineering the Reaction Pathway of a Non-heme Iron Oxygenase Using Ancestral Sequence Reconstruction. *J. Am. Chem. Soc.* **2024**, *146* (50), 34352−34363.
(165) Chesterfield, R. J.; Vickers, C. E.; Beveridge, C. A. Translation of Strigolactones from Plant Hormone to Agriculture: Achievements, Future Perspectives, and Challenges. *Trends Plant Sci.* **2020**, *25* (11), 1087−1106.
(166) Tokunaga, T.; Hayashi, H.; Akiyama, K. Medicaol, a strigolactone identified as a putative didehydro-orobanchol isomer, from *Medicago truncatula*. *Phytochemistry* **2015**, *111*, 91−97.
(167) Alder, A.; Jamil, M.; Marzorati, M.; Bruno, M.; Vermathen, M.; Bigler, P.; Ghisla, S.; Bouwmeester, H.; Beyer, P.; Al-Babili, S. The path from beta-carotene to carlactone, a strigolactone-like plant hormone. *Science* **2012**, *335* (6074), 1348−1351.
(168) Abe, S.; Sado, A.; Tanaka, K.; Kisugi, T.; Asami, K.; Ota, S.; Kim, H. I.; Yoneyama, K.; Xie, X.; Ohnishi, T.; Seto, Y.; Yamaguchi, S.; Akiyama, K.; Yoneyama, K.; Nomura, T. Carlactone is converted to carlactonoic acid by MAX1 in Arabidopsis and its methyl ester can directly interact with AtD14 in vitro. *Proc. Natl. Acad. Sci. U.S.A.* **2014**, *111* (50), 18084−18089.
(169) Zhang, Y.; van Dijk, A. D.; Scaffidi, A.; Flematti, G. R.; Hofmann, M.; Charnikhova, T.; Verstappen, F.; Hepworth, J.; van der Krol, S.; Leyser, O.; Smith, S. M.; Zwanenburg, B.; Al-Babili, S.; Ruyter-Spira, C.; Bouwmeester, H. J. Rice cytochrome P450 MAX1 homologs catalyze distinct steps in strigolactone biosynthesis. *Nat. Chem. Biol.* **2014**, *10* (12), 1028−33.
(170) Yoneyama, K.; Mori, N.; Sato, T.; Yoda, A.; Xie, X.; Okamoto, M.; Iwanaga, M.; Ohnishi, T.; Nishiwaki, H.; Asami, T.; Yokota, T.; Akiyama, K.; Yoneyama, K.; Nomura, T. Conversion of carlactone to carlactonoic acid is a conserved function of MAX1 homologs in strigolactone biosynthesis. *New Phytol.* **2018**, *218* (4), 1522−1533.
(171) Homma, M.; Wakabayashi, T.; Moriwaki, Y.; Shiotani, N.; Shigeta, T.; Isobe, K.; Okazawa, A.; Ohta, D.; Terada, T.; Shimizu, K.; Mizutani, M.; Takikawa, H.; Sugimoto, Y. Insights into stereoselective ring formation in canonical strigolactone: Identification of a dirigent domain-containing enzyme catalyzing orobanchol synthesis. *Proc. Natl. Acad. Sci. U.S.A.* **2024**, *121* (26), No. e2313683121.
(172) Gao, X.; Chooi, Y. H.; Ames, B. D.; Wang, P.; Walsh, C. T.; Tang, Y. Fungal indole alkaloid biosynthesis: genetic and biochemical investigation of the tryptoquialanine pathway in Penicillium aethiopicum. *J. Am. Chem. Soc.* **2011**, *133* (8), 2729−2741.
(173) Tao, H.; Ushimaru, R.; Awakawa, T.; Mori, T.; Uchiyama, M.; Abe, I. Stereoselectivity and Substrate Specificity of the Fe(II)/alpha-Ketoglutarate-Dependent Oxygenase TqaL. *J. Am. Chem. Soc.* **2022**, *144* (47), 21512−21520.
(174) Cha, L.; Paris, J. C.; Zanella, B.; Spletzer, M.; Yao, A.; Guo, Y.; Chang, W.-c. Mechanistic Studies of Aziridine Formation Catalyzed by Mononuclear Non-Heme Iron Enzymes. *J. Am. Chem. Soc.* **2023**, *145* (11), 6240−6246.
(175) Hou, X.; Sun, R.; Feng, Y.; Zhang, R.; Zhu, T.; Che, Q.; Zhang, G.; Li, D. Peptaibols: Diversity, bioactivity, and biosynthesis. *Eng. Microbiol.* **2022**, *2* (3), No. 100026.
(176) Zhang, X.; Liu, J.; Liao, L.; Wang, Z.; Wang, B. Coordination dynamics of iron enables the selective C−N coupling but bypasses unwanted C−H hydroxylation in Fe(II)/α-ketoglutarate- dependent non-heme enzymes. *Chin. J. Catal.* **2024**, *62*, 131−144.
(177) Sonawane, P. D.; Jozwiak, A.; Panda, S.; Aharoni, A. 'Hijacking'core metabolism: a new panache for the evolution of steroidal glycoalkaloids structural diversity. *Curr. Opin. Plant Biol.* **2020**, *55*, 118−128.
(178) Friedman, M. Tomato glycoalkaloids: role in the plant and in the diet. *J. Agric. Food Chem.* **2002**, *50* (21), 5751−5780.
(179) Friedman, M.; McDonald, G. M.; Filadelfi-Keszi, M. Potato glycoalkaloids: chemistry, analysis, safety, and plant physiology. *Crit. Rev. Plant Sci.* **1997**, *16* (1), 55−132.
(180) Cárdenas, P. D.; Sonawane, P. D.; Pollier, J.; Vanden Bossche, R.; Dewangan, V.; Weithorn, E.; Tal, L.; Meir, S.; Rogachev, I.; Malitsky, S.; et al. GAME9 regulates the biosynthesis of steroidal alkaloids and upstream isoprenoids in the plant mevalonate pathway. *Nat. Commun.* **2016**, *7* (1), 10654.
(181) Shakya, R.; Navarre, D. A. LC-MS analysis of solanidane glycoalkaloid diversity among tubers of four wild potato species and three cultivars (*Solanum tuberosum*). *J. Agric. Food Chem.* **2008**, *56* (16), 6949−6958.
(182) Iijima, Y.; Watanabe, B.; Sasaki, R.; Takenaka, M.; Ono, H.; Sakurai, N.; Umemoto, N.; Suzuki, H.; Shibata, D.; Aoki, K. Steroidal glycoalkaloid profiling and structures of glycoalkaloids in wild tomato fruit. *Phytochemistry* **2013**, *95*, 145−157.

https://doi.org/10.1021/acsbiomedchemau.5c00001
ACS Bio Med Chem Au 2025, 5, 238−261

(183) Itkin, M.; Heinig, U.; Tzfadia, O.; Bhide, A.; Shinde, B.; Cardenas, P.; Bocobza, S.; Unger, T.; Malitsky, S.; Finkers, R.; et al. Biosynthesis of antinutritional alkaloids in solanaceous crops is mediated by clustered genes. *Science* **2013**, *341* (6142), 175−179.
(184) Sonawane, P. D.; Heinig, U.; Panda, S.; Gilboa, N. S.; Yona, M.; Kumar, S. P.; Alkan, N.; Unger, T.; Bocobza, S.; Pliner, M.; et al. Short-chain dehydrogenase/reductase governs steroidal specialized metabolites structural diversity and toxicity in the genus Solanum. *Proc. Natl. Acad. Sci. U.S.A* **2018**, *115* (23), 5419−5428.
(185) McCue, K. F.; Shepherd, L. V.; Allen, P. V.; Maccree, M. M.; Rockhold, D. R.; Corsini, D. L.; Davies, H. V.; Belknap, W. R. Metabolic compensation of steroidal glycoalkaloid biosynthesis in transgenic potato tubers: using reverse genetics to confirm the in vivo enzyme function of a steroidal alkaloid galactosyltransferase. *Plant Science* **2005**, *168* (1), 267−273.
(186) McCue, K. F.; Allen, P. V.; Shepherd, L. V.; Blake, A.; Whitworth, J.; Maccree, M. M.; Rockhold, D. R.; Stewart, D.; Davies, H. V.; Belknap, W. R. The primary in vivo steroidal alkaloid glucosyltransferase from potato. *Phytochemistry* **2006**, *67* (15), 1590−1597.
(187) McCue, K. F.; Allen, P. V.; Shepherd, L. V.; Blake, A.; Maccree, M. M.; Rockhold, D. R.; Novy, R. G.; Stewart, D.; Davies, H. V.; Belknap, W. R. Potato glycosterol rhamnosyltransferase, the terminal step in triose side-chain biosynthesis. *Phytochemistry* **2007**, *68* (3), 327−334.
(188) Akiyama, R.; Watanabe, B.; Nakayasu, M.; Lee, H. J.; Kato, J.; Umemoto, N.; Muranaka, T.; Saito, K.; Sugimoto, Y.; Mizutani, M. The biosynthetic pathway of potato solanidanes diverged from that of spirosolanes due to evolution of a dioxygenase. *Nat. Commun.* **2021**, *12* (1), 1300.
(189) Sonawane, P. D.; Jozwiak, A.; Barbole, R.; Panda, S.; Abebie, B.; Kazachkova, Y.; Gharat, S. A.; Ramot, O.; Unger, T.; Wizler, G.; et al. 2-oxoglutarate-dependent dioxygenases drive expansion of steroidal alkaloid structural diversity in the genus Solanum. *New Phytol.* **2022**, *234* (4), 1394−1410.
(190) Srnec, M.; Iyer, S. R.; Dassama, L. M. K.; Park, K.; Wong, S. D.; Sutherlin, K. D.; Yoda, Y.; Kobayashi, Y.; Kurokuzu, M.; Saito, M.; Seto, M.; Krebs, C.; Bollinger, J. M., Jr.; Solomon, E. I. Nuclear Resonance Vibrational Spectroscopic Definition of the Facial Triad Fe(IV) horizontal lineO Intermediate in Taurine Dioxygenase: Evaluation of Structural Contributions to Hydrogen Atom Abstraction. *J. Am. Chem. Soc.* **2020**, *142* (44), 18886−18896.
(191) Matthews, M. L.; Krest, C. M.; Barr, E. W.; Vaillancourt, F. H.; Walsh, C. T.; Green, M. T.; Krebs, C.; Bollinger, J. M. Substrate-triggered formation and remarkable stability of the C-H bond-cleaving chloroferryl intermediate in the aliphatic halogenase, SyrB2. *Biochemistry* **2009**, *48* (20), 4331−4343.
(192) Matthews, M. L.; Neumann, C. S.; Miles, L. A.; Grove, T. L.; Booker, S. J.; Krebs, C.; Walsh, C. T.; Bollinger, J. M. Substrate positioning controls the partition between halogenation and hydroxylation in the aliphatic halogenase, SyrB2. *Proc. Natl. Acad. Sci. U.S.A.* **2009**, *106* (42), 17723−17728.

https://doi.org/10.1021/acsbiomedchemau.5c00001
ACS Bio Med Chem Au 2025, 5, 238−261